Major ion chemistry of the Yarlung Tsangpo–Brahmaputra river: Chemical weathering, erosion, and CO_2 consumption in the southern Tibetan plateau and eastern syntaxis of the Himalaya

Michael T. Hren [a,*], C. Page Chamberlain [a], George E. Hilley [a],
Peter M. Blisniuk [b], Bodo Bookhagen [a]

[a] *Stanford University, Department of Geological and Environmental Sciences, Stanford, CA 94305, USA*
[b] *Institut für Geowissenschaften, Universität Potsdam, Potsdam, Germany*

Abstract

The Yarlung Tsangpo–Brahmaputra river drains a large portion of the Himalaya and southern Tibetan plateau, including the eastern Himalayan syntaxis, one of the most tectonically active regions on the globe. We measured the solute chemistry of 161 streams and major tributaries of the Tsangpo–Brahmaputra to examine the effect of tectonic, climatic, and geologic factors on chemical weathering rates. Specifically, we quantify chemical weathering fluxes and CO_2 consumption by silicate weathering in southern Tibet and the eastern syntaxis of the Himalaya, examine the major chemical weathering reactions in the tributaries of the Tsangpo–Brahmaputra, and determine the total weathering flux from carbonate and silicate weathering processes in this region. We show that high precipitation, rapid tectonic uplift, steep channel slopes, and high stream power generate high rates of chemical weathering in the eastern syntaxis. The total dissolved solids (TDS) flux from the this area is greater than 520 tons km^{-2} yr^{-1} and the silicate cation flux more than 34 tons km^{-2} yr^{-1}. In total, chemical weathering in this area consumes 15.2×10^5 mol CO_2 km^{-2} yr^{-1}, which is twice the Brahmaputra average. These data show that 15–20% of the total CO_2 consumption by silicate weathering in the Brahmaputra catchment is derived from only 4% of the total land area of the basin. Hot springs and evaporite weathering provide significant contributions to dissolved Na^+ and Cl^- fluxes throughout southern Tibet, comprising more than 50% of all Na^+ in some stream systems. Carbonate weathering generates 80–90% of all dissolved Ca^{2+} and Mg^{2+} cations in much of the Yarlung Tsangpo catchment.
© 2007 Elsevier Ltd. All rights reserved.

1. INTRODUCTION

The Brahmaputra is the fifth largest river in the world (Berner and Berner, 1996), and is second only to the Yellow river in China in terms of sediment transported per unit area (Milliman and Meade, 1983). It is the single largest river system draining the Himalaya and southern Tibetan plateau and transports a significant portion of all physically and chemically weathered material in this region. In total, the Brahmaputra carries over 73 million tons of dissolved material annually, which accounts for approximately 4% of the total dissolved flux to the worlds oceans (Singh et al., 2005).

Recent measures of the dissolved chemical load and total sediment flux from a number of Himalayan rivers shows that the Brahmaputra exhibits significantly higher rates of physical and chemical weathering than other large Himalayan catchments (Sarin and Krishnaswami, 1984; Sarin et al., 1989; Harris et al., 1998; Galy and France-Lanord, 1999; Galy and France-Lanord, 2001; Dalai et al., 2002; Singh and France-Lanord, 2002; Singh et al., 2005). Spatially averaged chemical denudation rates in the Brahmaputra basin (∼105 tons km^{-2} yr^{-1}; Sarin et al., 1989) are 2–3 times

greater than the next largest Himalayan river, the Ganges (Galy and France-Lanord, 1999), and 5 times greater than the world average (Sarin et al., 1989). These high rates of chemical weathering result in the consumption of $\sim 6 \times 10^5$ mol km^{-2} yr^{-1} CO_2 due to the weathering of silicate minerals (Singh et al., 2005).

A number of authors have argued that high rates of chemical weathering in the Brahmaputra basin result from rapid rock uplift and heavy monsoonal precipitation which drives rapid physical erosion along the southern and eastern edge of the Himalaya (Sarin et al., 1989; Galy and France-Lanord, 2001). Indeed, throughout much of the Himalaya, physical erosion rates are some of the world's highest and reach 2.7 mm yr^{-1} in the High Himalaya and up to ~ 1.2 mm yr^{-1} on the southern edge of the Tibetan plateau (Vance et al., 2003). On the plateau itself, erosion rates may be significantly lower however (0.013 mm yr^{-1}) due to low precipitation (Lal et al., 2003). The eastern syntaxis of the Himalaya, which marks the eastern edge of the collision between the Indian and Eurasian plates, is characterized by particularly high rates of exhumation and erosion. Here rock uplift rates are some of the highest in the world (up to 10 mm/yr; Burg et al., 1998) and are in part driven by rapid river incision of the Brahmaputra and glacial removal of bedrock (Zeitler et al., 2001). These rapid rates of erosion are evidenced by a steep river profile, high erosive index, and elevated stream power (Finlayson et al., 2002). Sediments generated in this rapidly eroding portion of the drainage are shown to account for nearly 35–45% of the total sediment transported in the Brahmaputra and 20% of the total sediment reaching the Bay of Bengal (Singh and France-Lanord, 2002; Garzanti et al., 2004).

Modeling studies (Chamberlain et al., 2005; Waldbauer and Chamberlain, 2005) show that chemical weathering rates are expected to be high in regions of rapid surface uplift and erosion. Given the rapid exhumation of bedrock and extremely high rate of sediment generation in the eastern syntaxis, chemical weathering rates in this area of the Brahmaputra basin are expected to be significantly higher than other portions of the catchment. As a result, chemical weathering in this region may comprise a significant portion of the chemical budget of the Brahmaputra. At present, one data point (Singh et al., 2005) is used to suggest that rapid chemical weathering in the eastern syntaxis is responsible for the high dissolved chemical weathering fluxes in the Brahmaputra. From this data point, it is argued that chemical weathering in the eastern syntaxis dominates the total dissolved flux of the Brahmaputra, with localized chemical denudation rates of 300 tons km^{-2} yr^{-1} (Singh et al., 2005). In light of the significance of the Brahmaputra river on global sediment and chemical budgets, it is important to understand the dominant chemical weathering processes in this catchment, the spatial patterns of chemical denudation, and specifically, to determine whether small areas of a landscape can exert significant control on global chemical budgets. This is particularly relevant in light of recent arguments which suggest that Cenozoic climate change was driven by atmospheric CO_2 reduction resulting from accelerated silicate weathering due to the uplift of the Himalaya and Tibetan plateau (Raymo et al., 1988; Raymo and Ruddiman, 1992).

We collected a total of 161 water samples from the Yarlung Tsangpo–Brahmaputra and its tributaries in southern Tibet in 2004 and 2005 and from the Siang–Brahmaputra in 2006 to: (1) quantify the role of the eastern syntaxis on chemical weathering fluxes in the Brahmaputra river; (2) determine the proportions of carbonate and silicate weathering in the main tributaries of the Yarlung Tsangpo–Brahmaputra in southern Tibet; and (3) examine spatial patterns of CO_2 consumption by silicate weathering in different portions of this basin.

2. GEOLOGIC SETTING

2.1. The Yarlung Tsangpo–Brahmaputra and the Tibetan plateau

The Himalayan orogenic belt is a 2000 km long, east–west trending feature marking the collision of the Eurasian and Indian plates. At the western and eastern ends, the belt terminates at the Nanga Parbat and Namche Barwa syntaxes, areas that are characterized by exhumation rates of up to 10 mm yr^{-1} (Zeitler et al., 1993; Burg et al., 1998). In the eastern end of this collisional zone, the suture between the Eurasian and Indian plates follows an east–west trend identified as the Indus Tsangpo Suture Zone (Gansser, 1964; Gansser, 1980) and spans a clearly defined "indentor corner" at the edge of the Indian plate (Koons, 1995). Directly north of the ITSZ (Indus Tsangpo Suture Zone) the Tibetan plateau is underlain by the Lhasa block, which is dominated by 120–40 Ma Transhimalayan plutons consisting of gabbroic to granodioritic batholiths of the Gangdese belt (Zhang et al., 1981). Within the Lhasa block, calc-alkaline plutons intrude into a series of sedimentary rocks and Precambrian basement. South of the Transhimalayan plutonic belt, local bedrock is dominated by North Himalayan gneiss domes and intermixed Paleocene to Eocene conglomerates, shales, sandstones, and local basalt flows of the Tethys Himalayan zone (Burg and Chen, 1984) (Fig. 1).

2.2. Namche Barwa and the eastern syntaxis of the Himalaya

The eastern Himalayan syntaxis marks the zone where the fault systems related to the Eurasian/Indian plate suture change from an E–W trend to N–S trend and acts as the boundary between the Gangdese or Transhimalayan Plutonic Belt (formerly the Asian plate margin) and the Himalayan Tethys sediments (Fig. 1). This region is marked by the massive peaks of Gyala Peri (7281 m) and Namche Barwa (7756 m). At the core of the Namche Barwa syntaxis is a large north-plunging antiform which is rimmed to the north by a U-shaped shear zone system. Here, migmatitic gneisses have been exhumed over the last several million years and local bedrock records high grade metamorphism marked by granulite facies rocks (Ding and Zhong, 1999). In the immediate area of the syntaxis, young (U–Th)/He and U–Pb zircon ages and biotite Ar–Ar ages indicate rapid rates of uplift and exhumation (Booth et al., 2004; Malloy, 2004) accommodated by some of the most rapid rates of fluvial incision in the world. Estimates of exhumation rates for this
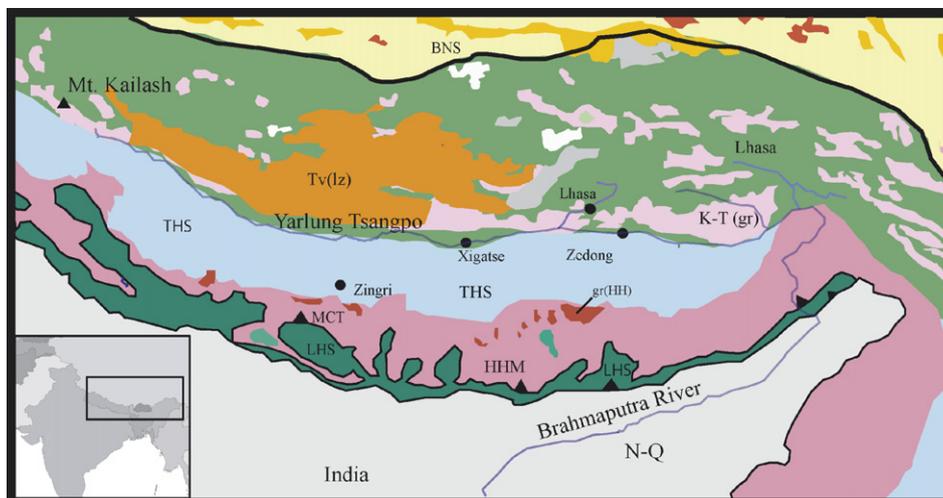
Fig. 1. Geologic map of the southern Tibetan plateau and eastern Himalayan syntaxis (modified from Yin and Harrison, 2000). The geologic units shown in the figure are as follows: HHM (High Himalayan Metamorphic series); LHS (Lesser Himalaya Metasediments); THS (Tethyan Himalayan Sequence); N-Q (Neogene-Quaternary Sediments); K-T(gr) (Cretaceous-Tertiary granitic plutons); gr(HH) (High Himalayan granites); Tv(lz) (Tertiary volcanics); MCT (Main Central Thrust); BNS (Bangong-Nujian Suture).

region range from 3 to 10 mm yr^{-1} over the last several million years (Burg and Meier, 1997; Burg et al., 1998).

3. CLIMATE, VEGETATION, AND HYDROLOGY OF THE YARLUNG TSANGPO–BRAHMAPUTRA

3.1. Hydrology and climate of the Yarlung Tsangpo–Brahmaputra

The Brahmaputra river carries approximately 2.7% of the total world freshwater discharge (Berner and Berner, 1996) and is the single greatest source of sediment to the oceans (Milliman and Meade, 1983). It serves as one of the primary drainages for all of the central and eastern Himalayas and southern Tibetan plateau, covering close to 630,000 km^2. The headwaters of the Yarlung Tsangpo, the main high Himalaya stem of the Brahmaputra river, originate at ~5200 m elevation at the base of the Chamyungdung glacier at Mount Kailash in south-central Tibet. From here, the Tsangpo flows due east for ~1300 km along the Indus–Tsangpo suture between the Indian and Eurasian plates. In the western portion of the Tsangpo basin, a strong rainshadow effect from the Himalayas shields the catchment from significant monsoonal rainfall and limits total precipitation to <0.3 m yr^{-1}. As a result, the Tsangpo discharge before the eastern syntaxis is less than 10% of the total Brahmaputra river flux in Bangladesh. At the far eastern end of the Himalayan belt, the river changes its E–W course and bends north around Namche Barwa. Here, the Tsangpo river slope becomes extreme, dropping approximately 2000 m in a distance of 200 km. In this area, yearly precipitation (>700 mm yr^{-1}) is greater than in western portions of the drainage and varies dramatically with elevation. Areas above snowline receive an equivalent of 2500–3000 mm of precipitation a year (Li and Zheng, 1981). South of the syntaxis, the Yarlung Tsangpo becomes the Siang, which joins the Dihang and Lohit river in the Assam plain at Pasighat to form the Brahmaputra,

ultimately joining the Ganges and draining to the Bay of Bengal. Here, discharge varies dramatically throughout the year, with the highest discharges occurring between June and October. Previous estimates of rainfall suggest that the three peak monsoon months of June to September accounts for 70–77% of total precipitation in the upper Yarlung Tsangpo (Guan and Chen, 1981), however TRMM satellite precipitation data (Bookhagen and Burbank, 2006) suggests that the eastern syntaxis region of the Himalaya may receive 50 percent or more of total yearly precipitation outside of the Indian Summer Monsoon.

In the eastern part of the Yarlung Tsangpo drainage near the Namche Barwa syntaxis, glaciers play an important part in shaping the local topography and likely exert significant control on the riverine chemistry of the two most heavily glaciated tributaries, the Yi'Ong Tsangpo and Parlung Tsangpo. Snow line for this area is at ~4500 to 4700 m, however the present lower extent of most glaciers in this region is ~5000–5200 m. In the vicinity of the syntaxis, glaciers cover nearly 8000 km^2 (Li and Zheng, 1981).

3.2. Physical erosion rates in the Yarlung Tsangpo–Brahmaputra basin

Exhumation and erosion rates in the Himalaya are extremely high, reaching 2.9 mm yr^{-1} in the eastern Himalaya and 2.1 mm yr^{-1} in the west (Galy and France-Lanord, 2001). In particular, the eastern syntaxis of the Himalaya exhibits some of the highest rates of exhumation on the globe (up to 10 mm yr^{-1}) (Burg et al., 1998). Here rapid rock uplift is accommodated by and possibly controlled by rapid incision of the Tsangpo–Brahmaputra and the resultant removal of large volumes of rock and sediment through glacial erosion and massive landsliding (Zeitler et al., 2001). As a result, this area generates a disproportionate percentage of the suspended sediment and dissolved chemical load and may account for 40% of the total Brahmaputra sediment flux

(Singh and France-Lanord, 2002; Singh et al., 2003; Garzanti et al., 2004; Singh et al., 2005).

4. SAMPLING AND CHEMICAL ANALYSIS

4.1. Stream solute chemistry

We sampled 144 streams and major Tibetan tributaries of the Yarlung Tsangpo–Brahmaputra (Figs. 2 and 3) and 17 tributaries along the Siang, south of the eastern Himalayan syntaxis (Fig. 3). Waters collected for dissolved Si and base cation analysis were filtered through 0.45 μm nylon filters into acid-washed HDPE bottles and acidified with double distilled nitric acid. Cation and dissolved Si concentrations in stream waters were measured using an Atomic Emission spectrometer (ICP-AES). Water samples for anion measurements were filtered through 0.45 μm nylon filters and collected in HDPE bottles. Alkalinity measurements were made by gran titration soon after sample collection. Anion concentrations were measured using a Dionex AS-4 ion-chromatograph. Measurement error for cation and anion analyses is within ±10%. Stream pH and temperature measurements were made with an Accument AP-61 pH meter and temperature probe on site. The estimated uncertainty for measurements is ±0.05 pH units and ±0.1 °C.

4.2. Composition of stream bedload

Few detailed geologic maps exist for the regions of the main tributaries of the Yarlung Tsangpo–Brahmaputra river in southern Tibet. As a result we examined the geologic makeup of the stream bedload using a pebble count to obtain a general understanding of the primary rock types represented within each drainage. At each stream sampling site, we collected a minimum of 50 rock samples at random from the main stream channel for hand identification. Most rocks in the stream bed-load fall into three major groups: granite/granitic gneiss, schist/other felsic volcanic, and mafic volcanics that includes amphibolites and other high-grade mafic metamorphics. Despite the abundance of carbonate in the Tethyan sediments and subordinate amounts of carbonate in the High Himalayan Crystalline units, little or no carbonate pebbles were observed in bedload samples upstream of the syntaxis region. Bedload composition data are shown in Appendix A.

4.3. Chemical flux measurements

To determine annual chemical weathering fluxes, it is necessary to have accurate stream discharge data. Due to a lack of stream gauging stations in southern Tibet, discharge estimates for this study are derived from calibrated Tropical Rainfall Measurement Mission (TRMM) satellite measurements averaged over the past 8 years (Bookhagen and Burbank, 2006). Rainfall-weighted flow accumulations were calculated using a patched 90 m Shuttle Radar Topography Mission (SRTM V2) digital elevation model. We observe that accumulated TRMM rainfall can be used to predict discharge along the Himalayan mountain front and in the eastern syntax (Finnegan et al., 2005; Anders et al., 2006). While runoff estimates based on satellite precipitation data provide a good measure of total discharge, these types of estimates do not necessarily take into account potential water losses through infiltration and evapotranspiration as well as discharge increase due to snowmelt. However, glacial coverage on the southern Tibetan Plateau is moderate and evapotranspiration is low due to the non-existent vegetation cover and
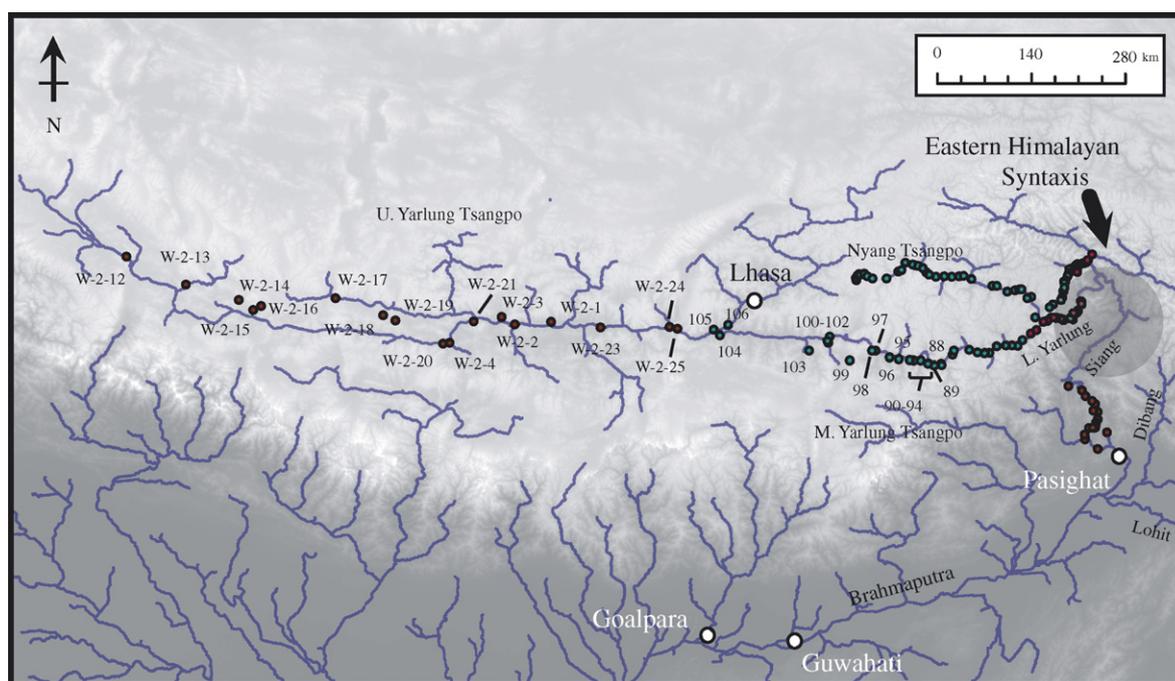
Fig. 2. Sample location map for the Yarlung Tsangpo–Brahmaputra river system. Sample locations and identifiers are shown for stream samples in the upper and middle Yarlung Tsangpo.
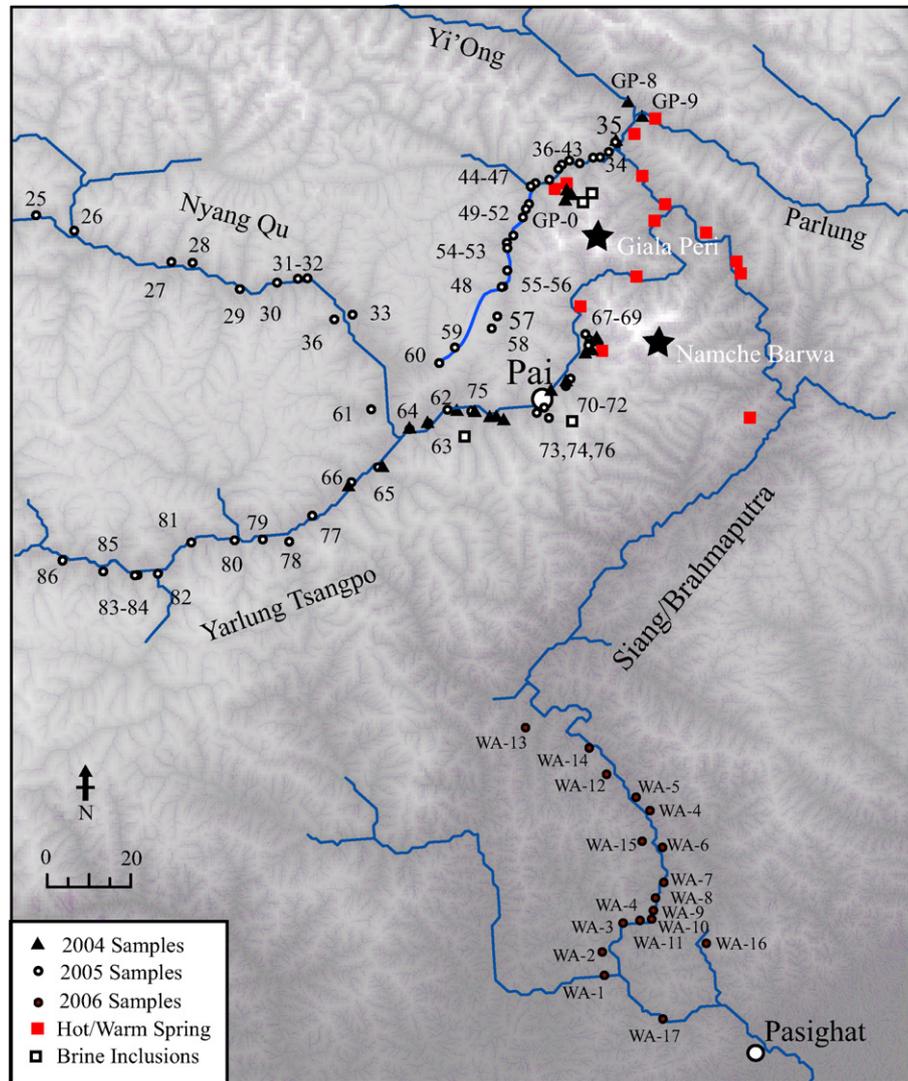
Fig. 3. Sample location map for the eastern syntaxis region. Unfilled circles indicate samples collected in 2005. Black triangles represent waters collected in 2004. Filled circles represent water samples from tributaries of the Siang south of the eastern syntaxis collected in February 2006. The locations of hot/warm springs (filled squares) and inactive hydrothermal systems (empty squares) with brine-inclusions (Taken from Craw et al., 2005) are also shown.

low mean annual temperatures. We argue that possible losses from the system add uncertainty to flow estimates that may range from 0% to 30% (whereby 30% indicates the maximum increase in discharge due to snowmelt at the southern Himalayan front). One comparable streamflow estimate is lower (locally up to 50% at Pai) than that used in previous studies of the Tsangpo–Brahmaputra (Singh et al., 2005). This may be due to increased glacial runoff or the difficulty in precisely estimating streamflow measurements in mountainous areas. Thus, although our absolute discharge amounts may vary from in situ measurements, the relative amounts are thought to be accurately represented.

In order to determine the amount of energy exposed per unit area, we use a specific stream power approach (Knighton, 1998). The specific stream power is defined as the gravity times the density of water times the energy slope (river gradient) times the discharge divided by the channel width. The channel slopes are extracted from the patched 90 m SRTM V2 digital elevation model, the discharge is given by the calibrated TRMM rainfall data, and we use a power-law relationship with discharge to derive channel width. We smooth the specific stream power profile over a sliding window of 20 km to rule out local disturbances.

5. RESULTS AND DISCUSSION

5.1. The solute chemistry of the Nyang, Po and Yarlung Tsangpo

The main drainages sampled in this study include the Nyang, Po, Yarlung Tsangpo, Lhasa He, and Siang (Figs. 2 and 3). Solute chemistry and chemical flux data for stream samples are grouped by drainage basin and distinguish small tributaries from main river stems. These data are shown in Table 1.

Table 1
Major ion composition of the Yarlung Tsangpo and tributaries

Sample	Latitude	Longitude	Sample date	pH	T (°C)	Ca^{2+} (μmol/L)	K^+ (μmol/L)	Mg^{2+} (μmol/L)	Na^+ (μmol/L)	SiO_2 (μmol/L)	Sr^{2+} (μmol/L)	Cl^- (μmol/L)	NO_3^- (μmol/L)	SO_4^{2-} (μmol/L)	HCO_3^- (μmol/L)	TDS (mg/L)
Nyang Tsangpo basin tributaries																
05-Tibet-1	29.8527	92.3336	Apr-05	3.7	1.9	816	22	887	79	197	1.2	—	—	—	—	—
05-Tibet-2	29.8745	92.3279	Apr-05	7.1	2.3	723	14	273	58	84	1.4	*B.D.*	10	726	540	146
05-Tibet-4	29.9006	92.3495	Apr-05	8.1	3.5	493	29	413	48	75	1.4	1	10	97	1720	151
05-Tibet-5*	29.9135	92.3658	Apr-05	7.5	5.2	427	32	275	230	98	1.0	96	7	237	1130	132
05-Tibet-6	29.9090	92.3822	Apr-05	7.6	4.3	423	21	197	68	87	1.0	*B.D.*	*B.D.*	98	1160	110
05-Tibet-7	29.0000	92.0000	Apr-05	7.4	5.2	271	24	117	55	91	0.5	19	6	81	680	72
05-Tibet-9	29.8908	92.4580	Apr-05	7.4	4.9	390	14	136	68	99	0.9	*B.D.*	10	90	1020	98
05-Tibet-10	29.8725	92.5229	Apr-05	7.4	5.1	391	14	101	57	102	0.7	*B.D.*	12	87	900	90
05-Tibet-11*	29.8737	92.6848	Apr-05	7.5	8.8	622	27	126	356	90	1.8	187	10	261	1220	149
05-Tibet-12	29.9443	92.8182	Apr-05	7.5	9.0	435	21	98	62	88	0.8	10	12	119	930	97
05-Tibet-13	29.9557	92.8580	Apr-05	7.5	9.0	432	34	162	51	81	0.7	*B.D.*	10	180	890	101
05-Tibet-14	30.0295	92.9007	Apr-05	7.3	11.7	481	30	221	111	92	0.8	45	13	437	580	114
05-Tibet-15	30.0052	93.0166	Apr-05	7.5	10.1	365	18	74	60	91	0.6	4	11	57	850	82
05-Tibet-16*	29.9344	93.1498	Apr-05	7.3	9.8	252	17	47	56	80	0.4	2	7	103	460	56
05-Tibet-17	29.9110	93.1723	Apr-05	7.3	9.5	306	20	49	166	99	0.6	63	12	136	590	76
05-Tibet-18	30.0130	92.9866	Apr-05	7.5	6.9	374	28	145	60	97	0.6	*B.D.*	11	135	840	92
05-Tibet-19	29.9996	93.0386	Apr-05	7.4	9.5	218	11	38	48	85	0.4	*B.D.*	11	49	460	50
05-Tibet-20	29.9758	93.1033	Apr-05	7.5	8.2	117	9	19	63	111	0.2	*B.D.*	8	7	310	34
05-Tibet-21	29.8886	93.2547	Apr-05	6.8	7.0	215	22	93	51	79	0.4	*B.D.*	9	135	410	56
05-Tibet-22*	29.8916	93.3513	Apr-05	7.3	7.9	331	24	80	164	93	0.7	48	10	139	670	82
05-Tibet-23	29.8889	93.4367	Apr-05	7.4	10.0	256	18	124	67	99	0.6	*B.D.*	11	131	610	72
05-Tibet-24	29.8904	93.5251	Apr-05	7.4	10.4	196	22	106	52	85	0.5	*B.D.*	11	113	480	58
05-Tibet-25	29.8979	93.5721	Apr-05	7.4	8.0	176	17	76	48	78	0.4	*B.D.*	9	94	400	49
05-Tibet-26	29.8645	93.6677	Apr-05	7.7	10.0	465	28	96	106	86	0.9	33	5	166	930	104
05-Tibet-27	29.7943	93.9051	Apr-05	7.6	13.2	127	13	38	55	88	0.3	1	14	48	310	38
05-Tibet-28	29.7925	93.9604	Apr-05	7.6	11.5	131	14	42	46	80	0.3	*B.D.*	7	54	300	37
05-Tibet-29	29.7337	94.0763	Apr-05	7.7	11.7	107	17	28	52	85	0.3	*B.D.*	13	44	250	32
05-Tibet-30	29.7473	94.1678	Apr-05	7.8	7.6	43	6	8	38	88	0.1	*B.D.*	7	2	140	17
05-Tibet-32	29.7555	94.2391	Apr-05	7.5	7.9	63	9	11	50	91	0.1	*B.D.*	4	5	180	22
05-Tibet-33	29.6776	94.3546	Apr-05	7.7	9.1	72	16	13	43	90	0.2	*B.D.*	1	11	210	24
05-Tibet-36	29.6662	94.3102	Apr-05	—	—	55	13	12	38	86	0.1	*B.D.*	4	16	160	21
05-Tibet-59	29.6017	94.6068	Apr-05	7.7	5.3	63	10	12	26	65	0.1	*B.D.*	*B.D.*	6	170	19
05-Tibet-60	29.5679	94.5659	Apr-05	7.6	5.0	63	11	13	32	77	0.2	*B.D.*	1	7	170	20
05-Tibet-61	29.4699	94.3984	Apr-05	7.6	9.5	67	16	15	33	77	0.2	*B.D.*	3	14	180	22
Nyang Tsangpo																
05-Tibet-3*	29.8745	92.3291	Apr-05	7.2	2.5	695	22	187	76	116	1.6	*B.D.*	6	565	700	139
05-Tibet-8*	29.9129	92.4233	Apr-05	7.8	7.3	466	49	242	466	140	1.1	226	10	303	1160	154
05-Tibet-31*	29.7568	94.2197	Apr-05	7.7	12.8	388	27	102	147	97	0.8	55	4	145	880	98
Po Tsangpo basin tributaries																
05-Tibet-35	30.0411	95.0126	Apr-05	—	—	641	78	90	74	87	2.1	12	5	292	1000	128
05-Tibet-37*	30.0201	94.9973	Apr-05	7.8	10.9	594	91	103	126	142	2.7	*B.D.*	2	377	840	129

05-Tibet-38	30.0089	94.9744	Apr-05	7.9	9.9	471	43	64	110	129	0.8	24	3	204	810	102
05-Tibet-39	30.0089	94.9578	Apr-05	7.9	—	357	61	66	45	108	1.5	*B.D.*	1	211	540	79
05-Tibet-40	29.9969	94.9239	Apr-05	8.0	10.0	552	70	88	75	118	1.2	10	1	223	1020	120
05-Tibet-41	30.0034	94.8965	Apr-05	8.2	10.7	603	84	68	71	143	0.9	*B.D.*	2	186	1170	129
05-Tibet-42*	29.9948	94.8811	Apr-05	8.2	9.9	1017	82	147	189	100	3.3	32	5	495	1540	201
05-Tibet-43	29.9866	94.8726	Apr-05	8.2	11.2	807	114	114	61	132	1.4	*B.D.*	9	248	1550	168
05-Tibet-44	29.9617	94.8470	Apr-05	8.1	11.2	513	73	76	71	126	1.1	*B.D.*	9	179	1000	113
05-Tibet-45	29.9561	94.8138	Apr-05	8.2	11.9	960	110	124	142	208	2.8	*B.D.*	*B.D.*	302	1770	198
05-Tibet-46	29.9484	94.8026	Apr-05	8.0	10.0	292	30	52	78	129	0.5	7	*B.D.*	157	470	68
05-Tibet-47	29.9491	94.8032	Apr-05	8.1	9.8	396	33	53	61	109	0.6	3	4	128	740	84
05-Tibet-48	29.7328	94.7269	Apr-05	7.6	4.5	132	22	38	60	120	0.3	5	*B.D.*	27	360	40
05-Tibet-49	29.7328	94.7269	Apr-05	7.8	4.5	58	13	13	51	81	0.2	*B.D.*	1	7	180	21
05-Tibet-50	29.9110	94.7973	Apr-05	7.6	7.4	255	36	29	71	141	0.3	*B.D.*	4	48	560	61
05-Tibet-51	29.8999	94.7901	Apr-05	7.7	5.0	256	42	33	97	175	0.4	1	*B.D.*	53	580	66
05-Tibet-52	29.8814	94.7844	Apr-05	7.6	10.0	156	20	21	55	123	0.2	*B.D.*	7	39	340	41
05-Tibet-53	29.8466	94.7557	Apr-05	7.7	6.3	151	14	24	60	126	0.4	*B.D.*	6	60	310	41
05-Tibet-54	29.8287	94.7412	Apr-05	7.7	6.7	93	14	13	68	137	0.2	*B.D.*	1	10	260	31
05-Tibet-55	29.8166	94.7418	Apr-05	7.7	7.4	102	24	32	98	219	0.3	*B.D.*	1	13	350	44
05-Tibet-56	29.7666	94.7394	Apr-05	7.8	6.4	105	16	17	47	96	0.2	*B.D.*	4	19	260	30
05-Tibet-57	29.6686	94.7139	Apr-05	7.7	2.8	48	11	12	32	78	0.2	*B.D.*	*B.D.*	10	140	18
05-Tibet-58	29.6419	94.6970	Apr-05	7.9	4.0	44	9	12	29	75	0.1	*B.D.*	*B.D.*	8	130	16
GP-0	29.9227	94.8896	May-04	—	—	661	43	70	36	74	1.9	15	4	984	—	—
GP-8*	30.0972	95.0663	May-04	—	—	567	72	241	128	111	2.6	41	19	321	—	—
GP-9	30.0972	95.0663	May-04	—	—	358	28	125	66	68	0.7	22	10	166	—	—

Po Tsangpo

05Tibet-34*	30.0405	95.0123	Apr-05	7.7	7.9	1453	167	335	137	179	16.7	8	*B.D.*	*B.D.*	1630	186

Lower Yarlung Tsangpo basin tributaries

05Tibet-63	29.4319	94.5379	Apr-05	7.1	9.0	437	27	57	53	180	0.6	2	*B.D.*	86	910	96
05Tibet-63a	29.4378	94.5447	May-04	—	—	242	19	35	34	126	0.4	9	6	59	—	—
05Tibet-64	29.4263	94.4931	Apr-05	8.2	9.8	451	31	67	58	133	0.6	3	3	134	850	95
04Tibet-64a	29.4264	94.4929	May-04	—	—	206	21	40	35	109	0.3	13	7	56	—	—
05Tibet-67	29.6162	94.9410	Apr-05	8.0	7.9	1064	109	175	212	313	1.2	1	*B.D.*	746	1220	221
04Tibet-67a	29.6163	94.9411	May-04	—	—	635	111	172	210	321	1.2	16	3	755	—	—
05Tibet-68	29.6064	94.9410	Apr-05	7.8	5.2	1191	137	222	105	179	1.6	—	—	—	860	124
04Tibet-68a	29.6065	94.9406	May-04	—	—	654	135	182	76	168	1.4	14	6	989	—	—
05Tibet-69	29.6013	94.9374	Apr-05	7.1	7.7	758	54	73	122	240	0.5	15	*B.D.*	492	800	148
05Tibet-69a	29.6013	94.9365	May-04	—	—	512	55	71	127	267	0.5	83	12	137	—	—
05Tibet-70	29.5449	94.8925	Apr-05	7.2	8.3	694	53	121	37	143	1.0	1	*B.D.*	400	840	132
05Tibet-71	29.5254	94.8898	Apr-05	7.2	6.9	137	25	46	36	142	0.1	1	*B.D.*	77	260	40
05Tibet-72	29.5145	94.8810	Apr-05	7.2	6.8	173	45	68	47	124	0.2	4	3	86	400	52
04Tibet-72a	29.5203	94.8817	May-04	—	—	300	27	132	226	81	0.8	74	10	147	—	—
05Tibet-73	29.4611	94.8288	Apr-05	7.1	9.2	363	45	107	51	164	0.3	13	2	165	660	87
05Tibet-74	29.4412	94.8326	Apr-05	7.4	10.3	382	31	82	65	163	0.3	43	3	201	560	85

Table 1 (*continued*)

Sample	Latitude	Longitude	Sample date	pH	T (°C)	Ca^{2+} (μmol/L)	K^+ (μmol/L)	Mg^{2+} (μmol/L)	Na^+ (μmol/L)	SiO_2 (μmol/L)	Sr^{2+} (μmol/L)	Cl^- (μmol/L)	NO_3^- (μmol/L)	SO_4^{2-} (μmol/L)	HCO_3^- (μmol/L)	TDS (mg/L)
05Tibet-75	29.4627	94.6502	Apr-05	7.9	7.9	340	25	68	43	118	0.4	6	*B.D.*	166	520	72
NB-8	29.5025	94.8426	May-04	—	—	262	47	102	48	159	0.2	15	8	212	—	—
NB-15	29.4427	94.7258	May-04	—	—	157	15	30	25	78	0.1	16	3	76	—	—
NB-16	29.4430	94.7043	May-04	—	—	182	22	47	25	86	0.2	16	4	159	—	—
NB-17	29.4509	94.6936	May-04	—	—	267	27	54	46	141	0.3	16	3	176	—	—
NB-18	29.4626	94.6444	May-04	—	—	208	20	45	41	89	0.3	64	8	142	—	—
NB-19a	29.4648	94.6103	May-04	—	—	323	26	139	237	81	0.9	84	9	156	—	—
Lower Yarlung Tsangpo																
05Tibet-62*	29.4632	94.5922	Apr-05	7.0	10.1	531	35	220	384	101	1.2	133	12	248	1320	153
NB-5b*	29.6013	94.9365	May-04	—	—	270	26	121	211	77	0.7	99	10	137	—	—
NB-18*	29.4626	94.6444	May-04	—	—	285	23	121	194	83	0.7	64	8	142	—	—
Middle Yarlung Tsangpo basin tributaries																
04Tibet-65a	29.3431	94.4156	May-04	—	—	142	13	22	21	67	0.2	13	7	56	—	—
05Tibet-65	29.3436	94.4162	Apr-05	7.1	9.2	274	20	42	38	100	0.3	7	4	131	410	58
04Tibet-66a	29.3080	94.3466	May-04	—	—	109	9	18	15	57	0.2	10	5	29	—	—
05Tibet-66	29.3077	94.3472	Apr-05	7.2	9.9	202	14	34	28	81	0.3	6	5	75	340	43
05Tibet-76	29.4573	94.8157	Apr-05	7.5	11.0	310	33	91	58	193	0.2	10	*B.D.*	167	530	78
05Tibet-77	29.2394	94.2477	Apr-05	7.1	7.8	110	14	31	36	80	0.2	12	8	37	260	32
05Tibet-78	29.1859	94.1913	Apr-05	7.2	7.9	131	10	27	19	59	0.1	*B.D.*	4	33	270	30
05Tibet-79	29.1908	94.1276	Apr-05	7.2	7.3	203	35	92	25	72	0.2	*B.D.*	5	46	540	54
05Tibet-80	29.1896	94.0588	Apr-05	7.5	9.5	144	22	28	45	104	0.2	4	4	29	330	38
05Tibet-81	29.1849	93.9523	Apr-05	7.5	7.1	119	19	36	44	136	0.2	*B.D.*	4	9	340	37
05Tibet-82	29.1185	93.8697	Apr-05	7.7	11.0	291	14	65	40	73	0.5	*B.D.*	2	128	490	61
05Tibet-84	29.1158	93.8103	Apr-05	7.6	9.6	101	22	25	41	97	0.2	*B.D.*	2	11	290	31
05Tibet-85	29.1251	93.7403	Apr-05	7.8	8.9	112	22	23	52	96	0.3	1	1	11	310	33
05Tibet-86	29.1483	93.6335	Apr-05	7.8	11.2	100	18	14	61	119	0.3	1	2	6	290	32
05Tibet-87	29.1040	93.4454	Apr-05	7.9	11.5	133	20	19	90	162	0.4	3	*B.D.*	7	380	42
05Tibet-89*	28.9996	93.3206	Apr-05	8.0	11.1	826	20	366	132	103	1.8	4	6	—	850	—
05Tibet-90*	28.9987	93.2337	Apr-05	8.1	10.2	1139	31	394	110	101	1.7	*B.D.*	*B.D.*	—	1180	—
05Tibet-91*	29.0128	93.1651	Apr-05	8.0	11.9	1092	11	322	142	117	1.4	30	*B.D.*	—	1090	—
05Tibet-92*	29.0442	93.0764	Apr-05	8.3	5.6	1289	9	525	239	91	4.6	11	5	—	2140	—
05Tibet-93*	29.0448	92.9994	Apr-05	8.0	6.8	1478	8	513	208	119	3.1	59	16	—	1520	—
05Tibet-95*	29.0633	92.8251	Apr-05	8.2	10.0	1125	10	454	304	129	3.6	43	21	—	1900	—
05Tibet-96*	29.0764	92.7221	Apr-05	7.8	7.1	1370	8	620	218	158	2.3	39	9	—	840	—
05Tibet-97*	29.1406	92.5613	Apr-05	8.1	10.7	953	7	356	399	145	2.7	155	14	642	1600	230
05Tibet-98*	29.1409	92.5186	Apr-05	7.9	9.2	946	8	342	231	105	2.7	38	24	469	1800	216
05Tibet-99*	29.0430	92.2632	Apr-05	8.1	8.7	985	8	334	222	109	2.8	3	20	591	1770	226
05Tibet-100*	29.2193	92.0144	Apr-05	8.3	8.3	1042	49	386	990	175	3.0	443	20	656	2130	296
05Tibet-101	29.2787	92.0265	Apr-05	8.1	10.6	493	29	72	111	150	0.9	16	27	142	1000	111
05Tibet-103*	29.1352	91.7949	Apr-05	8.2	14.8	1251	43	545	551	152	2.5	146	31	—	1280	—

Middle Yarlung Tsangpo river

05Tibet-83*	29.1170	93.8179	Apr-05	8.2	14.2	787	48	369	681	118	1.9	245	22	399	2070	240
05Tibet-88*	29.0079	93.3139	Apr-05	8.6	13.3	829	49	395	685	120	2.0	255	21	515	2030	251
05Tibet-94*	29.0490	92.9514	Apr-05	8.4	12.8	862	55	429	831	119	2.2	313	23	477	2370	276
05Tibet-102*	29.2358	92.0042	Apr-05	8.5	17.2	874	58	417	806	116	2.3	302	22	418	2450	275
05Tibet-104*	29.2770	90.7684	Apr-05	8.6	10.8	906	70	520	990	129	2.3	327	29	533	2620	307
05Tibet-105*	29.3324	90.6971	Apr-05	8.7	13.1	938	69	529	1021	133	2.6	341	26	559	2650	314
05Tibet-106*	29.3492	90.7590	Apr-05	8.0	10.0	684	40	194	350	78	1.5	177	9	180	1700	174

Upper Yarlung Tsangpo basin tributaries

W-2-2	29.3266	88.4075	Aug-05	6.88	—	630	13	77	101	148	0.9	28	10	491	500	118
W-2-3	29.3965	88.2570	Aug-05	6.94	—	546	15	69	83	102	1.0	16	22	289	690	104
W-2-4*	29.1139	87.6697	Aug-05	7.60	—	800	43	151	378	126	2.0	185	29	398	1220	175
W-2-5	29.3126	87.0385	Aug-05	7.73	—	892	21	101	130	144	2.0	18	19	49	1880	172
W-2-6*	31.5342	79.9818	Sep-05	7.30	—	928	23	473	82	113	1.7	60	26	437	1910	220
W-2-7*	31.4532	80.1417	Sep-05	7.66	—	2033	1100	2687	3114	228	10.6	760	51	4309	4220	976
W-2-13*	29.5433	84.6183	Sep-05	7.98	—	930	30	180	158	106	2.2	58	15	274	1910	199
W-2-14*	29.4272	85.2341	Sep-05	8.08	—	1848	25	509	380	108	9.5	30	18	1929	1420	377
W-2-15*	29.3347	85.4051	Sep-05	8.00	—	1441	8	940	187	101	7.1	10	18	1870	1370	356
W-2-16*	29.3782	85.4946	Sep-05	8.08	—	1787	13	1470	328	85	9.2	10	24	3040	1880	529
W-2-17*	29.5061	86.3408	Sep-05	7.97	—	2757	21	741	240	133	14.7	11	19	3551	1150	555
W-2-18*	29.3604	86.8967	Sep-05	7.81	—	1590	22	210	172	121	6.4	17	49	848	2120	295
W-2-19	29.3126	87.0385	Sep-05	7.95	—	989	20	118	146	151	2.5	12	25	72	2120	194
W-2-20	29.1047	87.5988	Sep-05	7.88	—	858	4	276	46	69	1.5	12	15	147	1910	178
W-2-21	29.3429	87.9339	Sep-05	7.48	—	996	22	88	125	130	3.4	13	16	454	1330	180
W-2-22	29.3685	88.8227	Sep-05	6.79	—	218	16	56	68	93	0.8	16	21	54	430	51
W-2-23	29.3277	89.3965	Sep-05	7.38	—	683	26	213	279	114	2.0	81	16	305	1260	157
W-2-24	29.3526	90.1902	Sep-05	6.90	—	403	26	86	240	144	1.5	37	21	107	900	101
W-2-25	29.3344	90.2804	Sep-05	7.15	—	257	31	52	147	136	0.8	19	13	24	680	70

Siang Tsangpo/Brahmaputra tributaries

WA-1	28.2365	94.9515	Feb-06	7.91	—	907	20	717	62	186	0.5	13	31	70	3350	281
WA-2	28.2880	94.9469	Feb-06	6.49	—	637	59	68	65	215	4.5	20	37	568	400	126
WA-3	28.3497	94.9992	Feb-06	7.15	—	213	9	276	143	333	0.4	15	22	11	1120	110
WA-4*	28.5925	95.0693	Feb-06	7.42	—	837	17	232	294	154	1.6	19	19	337	1770	198
WA-5	28.6224	95.0359	Feb-06	7.65	—	738	41	420	94	175	1.5	17	31	338	1720	194
WA-6	28.5120	95.0993	Feb-06	6.71	—	126	11	121	75	140	0.3	13	20	11	500	52
WA-7	28.4361	95.1007	Feb-06	6.94	—	253	20	134	133	183	0.7	19	37	43	730	80
WA-8	28.4030	95.0798	Feb-06	7.28	—	236	18	260	134	239	0.7	15	24	28	1040	102
WA-9	28.3753	95.0743	Feb-06	7.51	—	452	40	598	284	286	2.7	43	45	73	2270	208
WA-10	28.3568	95.0693	Feb-06	7.31	—	336	31	385	121	282	1.5	18	42	23	1550	144
WA-11*	28.3548	95.0408	Feb-06	7.39	—	468	16	310	208	206	1.3	11	3	95	1580	150
WA-12	28.6730	94.9644	Feb-06	7.25	—	557	20	331	70	132	4.3	19	20	305	1150	142
WA-13	28.7769	94.7682	Feb-06	7.30	—	139	35	52	87	164	0.5	20	16	43	420	51
WA-14	28.7305	94.9236	Feb-06	7.88	—	894	20	739	55	170	1.8	17	15	333	2770	268
WA-15	28.5260	95.0492	Feb-06	7.20	—	527	17	348	49	135	3.8	17	23	354	1120	144
WA-16	28.3022	95.2020	Feb-06	7.40	—	371	20	287	71	213	1.0	16	24	362	1180	146
WA-17	28.1405	95.0930	Feb-06	7.78	—	659	35	373	84	201	1.2	27	16	65	1990	180

Despite the large number of samples from varied geologic and tectonic environments, the chemical composition of stream waters analyzed in this study are generally dilute, with TDS (Total dissolved solids = $Ca^{2+} + Mg^{2+} + K^+ + Na^+ + SiO_2 + Cl^- + NO_3^- + SO_4^{2-} + HCO_3^-$ in mg/L) ranging from 16 to 356 mg/L. However, a number of streams in the upper Yarlung Tsangpo, which is defined as the area of the basin upstream of where the Lhasa He joins the Yarlung Tsangpo, exhibit high TDS of up to 976 mg/L and may reflect hydrothermal inputs or evaporite weathering in these drainages. In general however, solute data are in good agreement with previous measures of the dissolved chemical composition of the upper Tsangpo and Lhasa He (Singh et al., 2005). At the time of sampling, stream water temperatures ranged from ∼2 °C in the high elevation sample sites of the upper Nyang to ∼14 °C in the westernmost sample locations along the middle Yarlung Tsangpo, and displayed neutral to alkaline pH values (6.8–8.7). No temperature data are available for samples collected in the upper Yarlung or Siang.

A good measure of the quality of the data presented here is the charge balance (μeq) between total dissolved cations ($TZ^+ = Na^+ + K^+ + 2Mg^{2+} + 2Ca^{+2}$) and total dissolved anions ($TZ^- = Cl^- + NO_3^- + 2SO_4^{2-} + HCO_3^-$). For most stream waters analyzed, the charge balance between cations and anions [$(TZ^+ - TZ^-)/(TZ^+ + TZ^-)$] is generally better than 10% which is within the total combined analytical uncertainty for all measurements. The relative molar proportions of cations are shown in a ternary plot of Ca^{2+}, Mg^{2+}, and $Na^+ + K^+$ (Fig. 4). With the exception of the Siang, most stream waters cluster near the Ca^{2+} corner of the ternary diagram and trend toward Na + K inputs from silicate weathering, hot springs, or evaporite additions. On average, Ca^{2+} accounts for ∼50–60% of all cations on a molar basis, followed by Na+ (∼15–25%), Mg^{2+} (15–25%) and K+

(∼10%) (Table 1). In the Nyang, the relative proportions of Ca^{2+} and Mg^{2+} decrease from west to east while Na^+ and K^+ generally increase. In the Po Tsangpo tributaries and upper and lower Yarlung Tsangpo, Na^+ makes up a larger percentage of total cations on a molar basis, comprising nearly 40% of all cations in some drainages. In the upper Yarlung, Ca^{2+} and Mg^{2+} concentrations are highly variable (218–2073 and 52–2687 μM, respectively) and in one catchment (W-2-7), Na^+ concentrations exceed 3000 μM. Samples from tributaries along the Siang are shifted toward the Mg^{2+} corner of the ternary plot, which may result from the weathering of more Mg-rich bedrock and dolomites, or the loss of Ca^{2+} from the system by preferential precipitation of calcite over dolomite during fluvial transport.

A ternary plot of the HCO_3^-, $Cl^- + SO_4^{2-}$, and dissolved Si show that most waters are dominated by bicarbonate (Fig. 5). On average, it comprises 83% of anions on a molar basis, followed by SO_4^{2-} (15%), NO_3^- (5%) and Cl^- (0–5%). In the tributaries of the upper Yarlung Tsangpo and in the eastern syntaxis, waters are characterized by high Cl^- (10–760 μM) and SO_4^{2-} (310–4220 μM), which may be attributable to the presence of hot springs or evaporites. High sulfate concentrations may also be derived from the oxidation of pyrite or other sulfides (Ping et al., 2000). This is observed firsthand in one drainage (05-Tibet-1), which is marked by pyritic rocks, low stream pH, and active iron oxide formation. This is likely an important source of SO_4^{2-} in many of the streams analyzed, as suggested by the lack of correlation between Cl^- and SO_4^2. This suggests that for many drainages, the primary source of SO_4^{2-} is from oxidation of pyrite, as is seen in other parts of the High Himalaya (Galy and France-Lanord, 1999). In addition, most streams exhibit low SO_4^{2-}/Ca^{2+} ratios (∼0.3) which limits possible evaporite input.
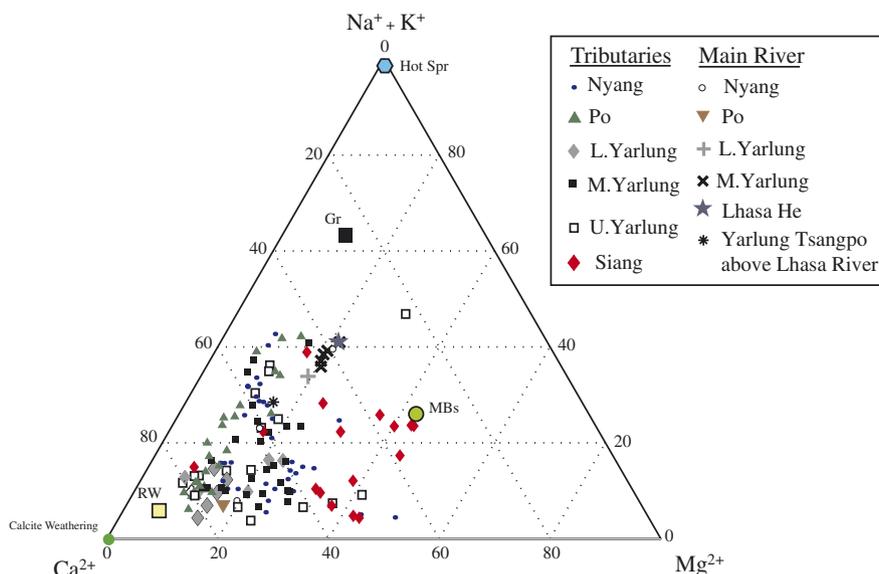
Fig. 4. Ternary plot of the dissolved Ca^{2+}, Mg^{2+}, and Na + K concentration of stream waters. Samples are identified as small tributaries or the main stem of each of these main rivers. Samples cluster near the Ca^{2+} endmember, highlighting the importance of weathering processes that release Ca^{2+}. The bulk composition of rainwater (RW), hot springs (Hot Spr), calcite, granite (Gr), and metabasalts (MBs) are shown.
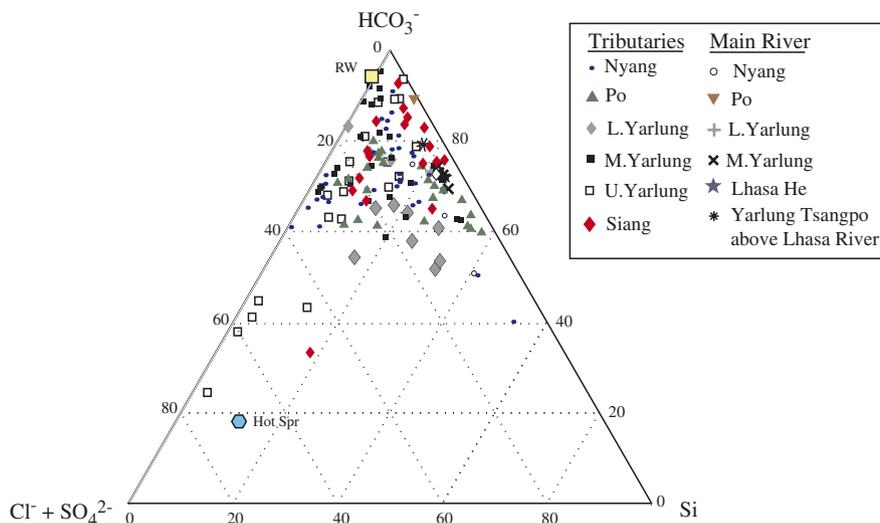
Fig. 5. Ternary plot of the dissolved HCO_3^-, SiO_2, and $Cl^- + SO_4^{2-}$ concentration of stream waters. Each symbol corresponds to streams from the main tributaries analyzed in this study, the Nyang, Po and lower and upper Yarlung. Samples are identified as small tributaries or the main stem of each of these main rivers. Stream waters cluster near the HCO_3^- endmember demonstrating that waters are governed by weathering processes that produce alkalinity. The bulk composition of rainwater (RW) and hot springs (Hot Spr) are shown.

5.2. Timing of stream sampling and flux estimates

We collected a number of samples from the same location in 2004 and 2005 to evaluate the year to year variability in dissolved solute concentrations. Solute measurements from the 2004 sampling are generally within 50% of the 2005 measures with the exception of Ca^{2+} and Mg^{2+}, which are up to 90% greater in 2005. This variability may result from greater stream discharge during the 2004 sampling due to higher snow melt and monsoonal precipitation in the May sampling period. In light of this variability, it is important to note that both April and May collection periods predate the peak monsoonal precipitation and runoff. Thus, subsequent interpretations fail to account for possible seasonal fluctuations in stream chemistry. In the lower Brahmaputra river, these seasonal variations in solute concentrations can be significant and measured concentrations vary between monsoonal and pre-monsoonal river flow (Chen and Guan, 1981; Sarin et al., 1989; Singh et al., 2005). Despite this, we submit that late April, May and August sampling periods may be used to generate reasonable annual flux estimates for the following reasons. First, recent chemical analyses of streams draining the High Himalaya show that during the monsoon, discharge increases by a factor of ~20 over winter flow, but total concentration is only slightly reduced (Galy and France-Lanord, 1999). Additionally, measurements of the seasonal variation of dissolved cations in the Yarlung Tsangpo at the Yangcun gauging station (1961), which is located close to sampling location 05-Tibet-100, shows a total annual variation in dissolved ion content from ~120 to 200 mg/L, with maximum concentrations occurring between November to April and minimum concentrations between June to September (Chen and Guan, 1981). Monthly measurements of stream discharge at this location show that October to May runoff contributes nearly 30% of the total annual discharge. Using monthly solute concentrations and total monthly discharge

(Chen and Guan, 1981) it is possible to calculate the estimated annual weathering flux using stream chemistry data from different monthly sampling periods. From this monthly record, we would predict that the total annual dissolved flux calculated from a single water analysis from mid-April or May would be 20–30% higher than calculated fluxes using monthly sampling or a single sample collected during peak stream discharge in late summer. Stream chemistry data from the lower Brahmaputra at Guwahati show that all major cations and dissolved Si concentrations in mid-April and May water samples are generally within 10–20% of June and July solute concentrations, and in some instances, mid-April or early May samples exhibit lower concentrations than mid-summer water samples (Singh et al., 2005). Thus, although late April and May sampling periods predate peak monsoonal precipitation and discharge, based on these published seasonal Brahmaputra stream chemistry data we would argue that the error induced by the timing of our stream sampling along the middle and lower Yarlung Tsangpo, Po Tsangpo, and Nyang Qu, is likely not greater 50%, which is roughly the maximum year to year variability in concentrations that we observed for most solutes.

Samples W-2-2 to W-2-25 in the upper Yarlung Tsangpo were collected in August of 2005 during peak discharge and as a result, flux estimates for these sites are likely more representative of the total yearly dissolved flux than measures based on water chemistry predating the monsoon. Samples WA-1 to WA-17 along the Siang river south of the eastern syntaxis were collected during February of 2006, which reflects the timing of the lowest stream discharges and highest solute concentrations in the Brahmaputra. As a result, chemical flux calculations for these sample sites may overestimate annual dissolved fluxes. However, TRMM satellite measurements (Bookhagen and Burbank, 2006) show that the eastern syntaxis region receives at least 50% of yearly precipitation outside of the Indian Summer Monsoon period. This

suggests that February stream chemistry for small tributaries in the vicinity of the syntaxis may be useful for calculating annual chemical fluxes.

5.3. Correction for atmospheric and hot-spring inputs to stream water dissolved ions

In some hydrologic systems, rainwater and atmospheric deposition of solutes can influence the cationic and anionic charge composition of stream waters. As a result, subtracting the contributions of these ions to a catchment is important when considering the stoichiometry of mineral weathering reactions, weathering fluxes, and the dominant weathering processes in a basin. In parts of the Himalaya, rain and snow can contribute a significant amount of dissolved solutes (Nijampurkar et al., 1993; Hasnain and Thayyen, 1999; Pandey et al., 2001). In the lower Brahmaputra, up to 30% of Na^+ may be derived from marine sources (Sarin and Krishnaswami, 1984). In contrast, in parts of the southern Tibetan plateau, atmospheric deposition of carbonate-rich dust may exceed 150 μg cm^{-2} yr^{-1} (Wake et al., 1994a) and can result in precipitation with highly variable quantities of dissolved cations or high ratios of dissolved Ca^{2+} to Cl^- (Wake et al., 1993; Wake et al., 1994b; Zhang et al., 2003). Given the large degree of spatial variability in potential atmospheric contributions to stream waters over the area of study, we use several approaches to correct for potential atmospheric and hydrothermal additions to stream waters.

One means of addressing the additions of dissolved cations and Cl^- from atmospheric sources is to multiply the measured molar concentration of each cation by the ion/Cl^- ratio measured in rainwater (Stallard and Edmond, 1981). Because the streams sampled in this study cover such a large area and different portions of the catchment receive different degrees of atmospheric inputs, we corrected for rainwater inputs by assuming that rainwater has the Cl^- content of the drainages with the lowest Cl^- concentration in each catchment. In tributaries of the Nyang Qu and the Po Tsangpo, greater than 60% of the drainages show no detectable Cl^- in solution. Although these concentrations are generally lower than would be expected from studies of Himalayan precipitation (Niehoff et al., 1994; Galy and France-Lanord, 1999; Ping et al., 2000) they are not considerably different from the low Cl^- concentrations (2.9 μM) measured in precipitation over the Tibet autonomous region (Table 2; Zhang et al., 2003). As a result, we assume that rain water additions to these two drainages are insignificant with the exception of Na^+ and Cl^-. Tributaries draining into the lower and middle Yarlung Tsangpo are corrected for the addition of rain water inputs using the measured ion/Cl^- ratio in precipitation in Lhasa (Table 2; Zhang et al., 2003) assuming rain has the Cl^- content of the lowest concentrations measured in these streams, which is ~1 μM Cl^-. For tributaries along the upper Yarlung Tsangpo and for samples of the main stem of the Yarlung Tsangpo, we assumed that rainwater had a Cl^- concentration of the stream with the lowest measured Cl^- concentration (10 μM) and corrected for rainwater inputs using ion/Cl- ratios in precipitation from Lhasa (Zhang et al., 2003). For tributaries of the Siang–Tsangpo, dissolved Cl^- concentrations are relatively constant over a large spatial extent and evaporites or hot springs are not believed to be significant sources of dissolved species. Here we corrected for atmospheric additions of dissolved cations using the measured ion/Cl^- ratio in precipitation collected at Goalpara and the measured Cl^- concentration in solution (Satsangi et al., 1998). Tables 3 and 4.

Many streams exhibit Cl^- concentrations in excess of what might be expected from additions by rainwater, reflecting possible additions from hot springs or evaporites. Hydrothermal systems can provide significant contributions to stream chemistry in active tectonic areas (Evans et al., 2001; Evans et al., 2004) and in the southern Tibetan plateau there are more than 600 known hydrothermal areas (Hui-xin, 1981; Si-yu and Ji-wen, 1981; Wei and Ming-Tao, 1981; Craw et al., 2005). These hydrothermal systems are part of the Himalayan geothermal belt and are primarily characterized by chloride- or sulfate-type fluids (Wei and Ming-Tao, 1981). A number of hot springs have been identified in the drainages around the Namche Barwa syntaxis (Craw et al.,

Table 2
Solute chemistry of precipitation in the Himalaya, Tibet and Yangbajin hot springs (in μmol/L)

Location	K^+	Na^+	Ca^{2+}	Mg^{2+}	Cl^-	NO_3^-	SO_4^{2-}	HCO_3^-
Lhasa 1998–2000[a]	5.14	11.2	197.4	10.9	9.7	6.9	5.2	231.7
Tibet Autonomic Region 1998–2000[a]	10.3	12.1	93.2	10.4	2.9	1.7	6	137
High Himalaya[b]	2	10	44	12	7	4	10	68
Goalpara[c]	4	21	153	94	38	43	19	44
Yangbajin hot springs[d]	58.8	403.5	4	0.1	562.1	ND	38.8	—
	K^+/Cl^-	Na^+/Cl^-	Ca^{2+}/Cl^-	Mg^{2+}/Cl^-		NO_3^-/Cl^-	SO_4^{2-}/Cl^-	HCO_3^-/Cl
Lhasa 1998–2000[a]	0.53	1.15	20.35	1.12	—	0.71	0.54	23.89
Tibet Autonomic Region 1998–2000[a]	3.55	4.17	32.14	3.59	—	0.59	2.07	47.24
High Himalaya[b]	0.29	1.43	6.29	1.71	—	0.57	1.43	9.71
Goalpara[c]	0.11	0.55	4.03	2.47	—	1.13	0.50	1.16
Yangbajin Hot Springs[d]	0.10	0.73	0.007	0.00	—	—	0.07	—

[a] Zhang et al. (2003).
[b] Galy and France-Lanord (1999).
[c] Satsangi et al. (1998).
[d] Ping et al. (2000) (Average hot spring values).

Table 3
Chemical weathering fluxes for the Yarlung Tsangpo and tributaries

Sample	Elevation (m)	Drainage area (km²)	Discharge (L/yr)	Carbonate weathering index	CWR_{Carb} (tons/km² yr)	$CWR_{Hot\ spring}$ (tons/km² yr)	CWR_{Sil} (tons/km² yr)	F_{SiO_2} (10^5 mol/km² yr)	$Flux_{Cations}$ silicate (10^5 mol/km² yr)	F_{CO_2} silicate (10^5 mol/km² yr)
Nyang Tsangpo basin tributaries										
05-Tibet-1	4729	5.8	9.81E+08	0.96	8.76	0.0	0.85	0.33	0.29	0.40
05-Tibet-2	4639	28.8	4.87E+09	0.95	5.73	0.0	0.60	0.14	0.20	0.29
05-Tibet-4	4527	6.5	8.33E+08	0.96	3.65	0.0	0.45	0.10	0.15	0.20
05-Tibet-5[a]	4450	162.2	2.33E+10	0.94	3.21	0.3	0.50	0.14	0.16	0.22
05-Tibet-6	4428	31.6	3.42E+09	0.91	2.14	0.0	0.47	0.09	0.16	0.22
05-Tibet-7	4369	79.0	1.11E+10	0.91	1.76	0.1	0.43	0.13	0.14	0.19
05-Tibet-9	4296	60.5	7.99E+09	0.89	2.24	0.0	0.54	0.13	0.18	0.26
05-Tibet-10	4220	20.0	2.67E+09	0.90	2.19	0.0	0.47	0.14	0.16	0.22
05-Tibet-11[a]	3982	732.0	8.60E+10	0.95	3.13	0.5	0.32	0.11	0.11	0.15
05-Tibet-12	3824	333.9	4.48E+10	0.91	2.44	0.0	0.49	0.12	0.16	0.22
05-Tibet-13	3780	63.2	1.05E+10	0.93	3.28	0.0	0.67	0.13	0.21	0.29
05-Tibet-14	3673	322.7	6.20E+10	0.90	4.29	0.2	0.99	0.18	0.33	0.46
05-Tibet-15	3600	160.0	2.57E+10	0.89	2.38	0.0	0.59	0.15	0.20	0.27
05-Tibet-16[a]	3500	74.4	1.25E+10	0.89	1.69	0.0	0.46	0.13	0.15	0.21
05-Tibet-17	3462	147.1	2.42E+10	0.71	1.63	0.2	1.12	0.16	0.39	0.56
05-Tibet-18	3624	17.6	3.87E+09	0.90	3.68	0.0	0.92	0.21	0.30	0.41
05-Tibet-19	3645	33.3	6.31E+09	0.84	1.56	0.0	0.56	0.16	0.19	0.27
05-Tibet-20	3568	9.7	1.37E+09	0.61	0.47	0.0	0.51	0.16	0.18	0.25
05-Tibet-21	3420	68.7	1.24E+10	0.86	1.70	0.0	0.64	0.14	0.21	0.29
05-Tibet-22[a]	3371	1628.1	2.38E+11	0.90	2.03	0.1	0.47	0.14	0.16	0.21
05-Tibet-23	3333	133.9	2.76E+10	0.85	2.34	0.0	0.87	0.20	0.29	0.41
05-Tibet-24	3300	63.2	1.05E+10	0.86	1.48	0.0	0.59	0.14	0.20	0.27
05-Tibet-25	3273	39.3	6.04E+09	0.84	1.15	0.0	0.49	0.12	0.16	0.22
05-Tibet-26	3224	3849.0	1.05E+12	0.88	5.06	0.2	1.43	0.23	0.48	0.67
05-Tibet-27	3150	86.4	1.86E+10	0.72	0.96	0.0	0.72	0.19	0.24	0.34
05-Tibet-28	3138	68.8	1.29E+10	0.77	0.92	0.0	0.56	0.15	0.19	0.26
05-Tibet-29	3148	159.8	3.10E+10	0.67	0.66	0.0	0.66	0.16	0.22	0.31
05-Tibet-30	3116	33.5	6.54E+09	0.36	0.16	0.0	0.44	0.17	0.15	0.21
05-Tibet-32	3070	170.8	3.22E+10	0.42	0.25	0.0	0.56	0.17	0.19	0.27
05-Tibet-33	3004	303.0	5.11E+10	0.57	0.33	0.0	0.48	0.15	0.16	0.22
05-Tibet-36	3136	232.1	4.11E+10	0.52	0.25	0.0	0.44	0.15	0.15	0.21
05-Tibet-59	4155	25.3	4.34E+09	0.71	0.35	0.0	0.30	0.11	0.10	0.14
05-Tibet-60	3508	52.6	1.04E+10	0.65	0.38	0.0	0.41	0.15	0.14	0.19
05-Tibet-61	2964	310.0	4.87E+10	0.65	0.32	0.0	0.37	0.12	0.12	0.17
Nyang Tsangpo										
05-Tibet-3[a]	4636	40.4	6.52E+09	0.94	4.96	0.0	0.63	0.19	0.21	0.29
05-Tibet-8[a]	4369	306.5	4.59E+10	0.92	3.36	0.7	0.71	0.21	0.24	0.33
05-Tibet-31[a]	3051	15974.0	3.07E+12	0.92	3.20	0.2	0.66	0.19	0.22	0.30

Table 3 (*continued*)

Sample	Elevation (m)	Drainage area (km^2)	Discharge (L/yr)	Carbonate weathering index	CWR$_{Carb}$ (tons/km^2 yr)	CWR$_{Hot\ spring}$ (tons/km^2 yr)	CWR$_{Sil}$ (tons/km^2 yr)	F_{SiO_2} (10^5 mol/km^2 yr)	Flux$_{Cations}$ silicate (10^5 mol/km^2 yr)	F_{CO_2} silicate (10^5 mol/km^2 yr)
Po Tsangpo basin tributaries										
05-Tibet-35	—	86.4	3.74E+10	0.92	11.25	0.1	2.79	0.38	0.86	1.10
05-Tibet-37[a]	2150	23.4	1.01E+10	0.91	10.51	0.0	3.15	0.61	0.96	1.22
05-Tibet-38	—	1.1	3.31E+08	0.85	5.58	0.2	2.03	0.41	0.67	0.92
05-Tibet-39	2228	8.7	3.13E+09	0.91	5.24	0.0	1.70	0.39	0.52	0.66
05-Tibet-40	2350	14.3	5.00E+09	0.91	7.80	0.1	2.19	0.41	0.68	0.88
05-Tibet-41	2408	8.5	3.03E+09	0.91	8.44	0.0	2.49	0.51	0.77	0.98
05-Tibet-42[a]	2408	35.4	1.19E+10	0.96	14.36	0.2	1.91	0.34	0.58	0.72
05-Tibet-43	2426	4.0	1.74E+09	0.94	14.69	0.0	3.37	0.58	1.00	1.23
05-Tibet-44	2481	10.2	4.21E+09	0.90	8.38	0.0	2.71	0.52	0.84	1.09
05-Tibet-45	2522	2.6	1.22E+09	0.89	17.23	0.0	5.41	0.96	1.72	2.28
05-Tibet-46	2510	826.5	3.29E+11	0.82	4.32	0.1	1.98	0.52	0.65	0.90
05-Tibet-47	2508	1713.3	4.34E+11	0.89	3.91	0.0	1.10	0.28	0.36	0.49
05-Tibet-48	3324	195.3	5.62E+10	0.71	1.30	0.0	1.10	0.35	0.37	0.50
05-Tibet-49	3324	175.8	4.90E+10	0.38	0.32	0.0	0.88	0.23	0.30	0.42
05-Tibet-50	2697	4.8	3.04E+09	0.79	5.60	0.0	3.22	0.89	1.05	1.44
05-Tibet-51	2730	2.9	1.72E+09	0.72	4.81	0.0	3.91	1.02	1.29	1.77
05-Tibet-52	2851	21.7	8.95E+09	0.74	2.13	0.0	1.52	0.51	0.51	0.70
05-Tibet-53	—	37.9	1.52E+10	0.71	1.95	0.0	1.48	0.51	0.50	0.71
05-Tibet-54	—	32.5	1.38E+10	0.46	0.88	0.0	1.73	0.58	0.59	0.84
05-Tibet-55	3113	3.5	1.44E+09	0.38	0.83	0.0	2.54	0.91	0.86	1.21
05-Tibet-56	3318	83.7	2.84E+10	0.67	1.10	0.0	1.05	0.33	0.35	0.49
05-Tibet-57	3679	8.8	2.33E+09	0.56	0.35	0.0	0.55	0.21	0.18	0.26
05-Tibet-58	3991	10.3	2.26E+09	0.56	0.27	0.0	0.42	0.16	0.14	0.19
GP-0	—	66.5	4.55E+10	0.96	18.60	0.0	2.44	0.51	0.75	0.96
GP-8[a]	—	9356.0	2.43E+12	0.94	7.02	0.0	1.49	0.29	0.46	0.58
GP-9	—	13592.0	1.46E+12	0.88	1.66	0.0	0.49	0.07	0.16	0.22
Po Tsangpo										
05Tibet-34[a]	2000	26498.0	5.87E+12	0.96	14.12	0.0	2.48	0.40	0.74	0.90
Lower Yarlung Tsangpo basin tributaries										
05Tibet-63	2940	31.3	5.84E+09	0.91	3.10	0.0	0.69	0.34	0.224	0.30
05Tibet-63a	—	31.3	5.84E+09	0.89	1.63	0.0	0.45	0.24	0.14	0.20
05Tibet-64	2955	51.3	1.27E+10	0.90	4.25	0.0	1.01	0.33	0.33	0.45
04Tibet-64a	—	51.3	1.27E+10	0.89	1.86	0.0	0.57	0.27	0.18	0.25
05Tibet-67	2980	22.0	1.79E+10	0.85	32.48	0.0	12.41	2.55	4.05	5.51
04Tibet-67a	—	22.0	1.79E+10	0.79	18.73	0.3	11.87	2.61	3.86	5.23
05Tibet-68	2912	37.9	2.47E+10	0.94	32.18	0.0	7.05	1.17	2.15	2.73
04Tibet-68a	—	37.9	2.47E+10	0.93	18.19	0.2	5.63	1.10	1.66	2.02
05Tibet-69	2869	54.5	3.15E+10	0.88	16.24	0.2	4.53	1.39	1.49	2.03
05Tibet-69a	—	54.5	3.15E+10	0.90	11.26	1.0	3.05	1.54	0.97	1.30
05Tibet-70	3130	13.6	3.52E+09	0.96	7.46	0.0	1.04	0.37	0.31	0.40
05Tibet-71	3003	9.6	1.97E+09	0.81	0.97	0.0	0.58	0.29	0.19	0.25
05Tibet-72	2935	41.3	7.92E+09	0.83	1.24	0.0	0.77	0.24	0.24	0.31

04Tibet-72a	—	41.3	7.92E+09	0.64	1.80	0.3	1.87	0.16	0.65	0.93
05Tibet-73	2941	10.1	3.18E+09	0.92	4.75	0.1	1.21	0.51	0.37	0.48
05Tibet-74	2954	58.0	1.41E+10	0.94	3.76	0.2	0.67	0.40	0.21	0.28
05Tibet-75	2946	118.1	2.88E+10	0.92	3.25	0.0	0.71	0.29	0.23	0.31
NB-8	—	1.2	2.80E+08	0.91	2.58	0.1	0.85	0.37	0.26	0.33
NB-15	—	78.0	2.21E+10	0.94	1.64	0.1	0.33	0.22	0.10	0.13
NB-16	—	10.0	3.51E+09	0.95	2.53	0.1	0.51	0.30	0.15	0.19
NB-17	—	77.7	1.86E+10	0.90	2.43	0.1	0.66	0.34	0.21	0.28
NB-18	—	118.1	2.88E+10	1.00	2.09	0.3	0.13	0.22	0.03	0.03
NB-19[a]	—	1.1	3.71E+08	0.92	5.04	0.6	0.99	0.29	0.33	0.45
Lower Yarlung Tsangpo										
05Tibet-62[a]	2900	205000.0	2.97E+13	0.92	2.42	0.4	0.48	0.15	0.16	0.22
NB-5b[a]	2900	205000.0	2.97E+13	0.81	0.61	0.3	0.36	0.11	0.12	0.17
NB-18[a]	—	204282.0	2.82E+13	0.82	0.65	0.2	0.36	0.11	0.12	0.17
Middle Yarlung Tsangpo basin tributaries										
04Tibet-65a	—	220.6	3.57E+10	0.93	0.82	0.0	0.16	0.11	0.05	0.07
05Tibet-65	2955	220.6	3.57E+10	0.91	1.66	0.0	0.39	0.16	0.13	0.17
04Tibet-66a	—	85.0	1.50E+10	0.94	0.66	0.0	0.13	0.10	0.04	0.05
05Tibet-66	2942	85.0	1.50E+10	0.91	1.30	0.0	0.30	0.14	0.10	0.13
05Tibet-76	2940	20.3	4.89E+09	0.89	2.97	0.0	0.94	0.46	0.30	0.40
05Tibet-77	2940	89.5	1.84E+10	0.81	0.73	0.0	0.38	0.16	0.13	0.17
05Tibet-78	2942	614.8	1.84E+11	0.89	1.36	0.0	0.39	0.18	0.13	0.17
05Tibet-79	2981	27.2	6.82E+09	0.93	2.21	0.0	0.65	0.18	0.20	0.25
05Tibet-80	2974	140.7	2.48E+10	0.76	0.77	0.0	0.53	0.18	0.17	0.24
05Tibet-81	2970	59.7	1.22E+10	0.73	0.73	0.0	0.60	0.28	0.20	0.27
05Tibet-82	2960	1580.0	1.82E+11	0.90	1.30	0.0	0.29	0.08	0.10	0.14
05Tibet-84	2975	49.6	7.55E+09	0.67	0.40	0.0	0.45	0.15	0.15	0.20
05Tibet-85	2994	79.8	1.24E+10	0.62	0.42	0.0	0.54	0.15	0.18	0.25
05Tibet-86	2997	115.3	2.12E+10	0.45	0.32	0.0	0.70	0.22	0.24	0.33
05Tibet-87	3033	99.0	1.55E+10	0.43	0.38	0.0	0.83	0.25	0.28	0.40
05Tibet-89[a]	3038	952.0	1.20E+11	0.96	5.01	0.0	0.43	0.13	0.14	0.20
05Tibet-90[a]	3061	64.9	1.30E+10	0.97	10.60	0.0	0.76	0.20	0.25	0.33
05Tibet-91[a]	3056	48.1	1.35E+10	0.96	13.75	0.2	0.94	0.33	0.33	0.46
05Tibet-92[a]	3101	617.2	1.08E+11	0.98	10.91	0.0	0.47	0.16	0.16	0.23
05Tibet-93[a]	3102	78.4	2.08E+10	0.97	18.36	0.3	0.85	0.32	0.30	0.43
05Tibet-95[a]	3143	708.0	1.67E+11	0.96	12.60	0.2	0.85	0.31	0.29	0.42
05Tibet-96[a]	3161	133.9	4.24E+10	0.97	21.16	0.2	1.35	0.50	0.47	0.69
05Tibet-97[a]	3265	546.5	1.56E+11	0.95	12.52	0.9	1.00	0.41	0.36	0.54
05Tibet-98[a]	3287	342.0	1.01E+11	0.96	12.89	0.2	0.86	0.31	0.30	0.43
05Tibet-99[a]	4081	73.5	1.59E+10	0.96	9.80	0.0	0.68	0.24	0.23	0.33
05Tibet-100[a]	3552	2035.3	3.61E+11	0.95	8.45	1.6	0.87	0.31	0.30	0.43
05Tibet-101	3592	270.8	3.70E+10	0.86	2.46	0.0	0.80	0.20	0.27	0.38
05Tibet-103[a]	3634	1066.0	1.98E+11	0.96	11.19	0.6	0.95	0.28	0.31	0.43
Middle Yarlung Tsangpo river										
05Tibet-83[a]	2961	147605.0	2.48E+13	0.95	5.09	0.8	0.66	0.20	0.22	0.31
05Tibet-88[a]	3012	143532.0	2.42E+13	0.95	5.50	0.8	0.68	0.20	0.22	0.31
05Tibet-94[a]	3101	141046.0	2.37E+13	0.95	5.83	1.0	0.67	0.20	0.22	0.31

Table 3 (*continued*)

Sample	Elevation (m)	Drainage area (km^2)	Discharge (L/yr)	Carbonate weathering index	CWR$_{Carb}$ (tons/km^2 yr)	CWR$_{Hot\ spring}$ (tons/km^2 yr)	CWR$_{Sil}$ (tons/km^2 yr)	F_{SiO_2} (10^5 mol/km^2 yr)	Flux$_{Cations}$ silicate (10^5 mol/km^2 yr)	F_{CO_2} silicate (10^5 mol/km^2 yr)
05Tibet-102[a]	3547	131797.0	2.21E+13	0.95	5.86	1.0	0.69	0.20	0.23	0.31
05Tibet-104[a]	3579	122484.0	2.06E+13	0.95	6.47	1.1	0.80	0.22	0.26	0.35
05Tibet-105[a]	3586	122359.0	1.47E+13	0.95	4.82	0.8	0.58	0.16	0.19	0.26
05Tibet-106[a]	3588	32779.0	5.81E+12	0.95	3.99	0.6	0.50	0.14	0.16	0.22
Upper Yarlung Tsangpo tributaries										
W-2-2	3905	30.3	4.95E+09	0.87	2.69	0.1	0.69	0.24	0.24	0.35
W-2-3	3979	71.0	8.95E+09	0.86	1.66	0.0	0.49	0.13	0.17	0.24
W-2-4[a]	3997	1595.0	2.01E+11	0.93	3.20	0.5	0.52	0.16	0.17	0.24
W-2-5	4502	145.2	2.66E+10	0.88	4.85	0.0	1.18	0.26	0.41	0.58
W-2-6[a]	4490	92.5	3.94E+09	0.96	1.64	0.0	0.15	0.05	0.05	0.07
W-2-7[a]	4762	21.2	1.39E+09	0.98	8.82	1.0	3.01	0.15	0.81	0.87
W-2-12	4606	22085.6	1.29E+12	0.67	0.32	0.0	0.35	0.08	0.12	0.17
W-2-13[a]	4607	678.6	8.19E+10	0.95	3.82	0.1	0.43	0.13	0.14	0.20
W-2-14[a]	4706	628.8	5.46E+10	0.98	6.64	0.0	0.31	0.09	0.10	0.14
W-2-15[a]	4528	40.1	4.21E+09	0.98	7.42	0.0	0.29	0.11	0.10	0.15
W-2-16[a]	4636	138.6	1.41E+10	0.99	9.94	0.0	0.26	0.09	0.09	0.12
W-2-17[a]	4741	192.3	1.80E+10	0.98	11.04	0.0	0.38	0.12	0.13	0.18
W-2-18[a]	4571	21.9	4.80E+09	0.97	12.84	0.0	0.83	0.27	0.28	0.39
W-2-19	4502	145.2	2.66E+10	0.87	5.53	0.0	1.39	0.28	0.48	0.69
W-2-20	4063	829.4	9.18E+10	0.97	3.51	0.0	0.19	0.08	0.07	0.10
W-2-21	3995	38.9	5.53E+09	0.89	4.32	0.0	0.92	0.18	0.32	0.45
W-2-22	3865	333.0	5.24E+10	0.26	0.03	0.0	0.49	0.15	0.17	0.24
W-2-23	3805	152.3	2.38E+10	0.73	2.79	0.2	1.85	0.18	0.65	0.93
W-2-24	3713	164.5	2.15E+10	0.35	0.48	0.1	1.52	0.19	0.53	0.76
W-2-25	3742	2378.0	3.42E+11	—	—	0.0	1.12	0.20	0.38	0.54
Siang Tsangpo/Brahmaputra tributaries[b]										
WA-1	395	3.0	2.37E+09	0.96	38.88	0.0	2.85	1.48	1.02	1.46
WA-2	265	4.2	3.26E+09	0.90	16.01	0.0	3.98	1.69	1.30	1.73
WA-3	340	8.7	8.55E+09	0.66	7.13	0.0	7.18	3.27	2.72	4.05
WA-4[a]	326	16.5	2.21E+10	0.92	43.44	0.0	6.21	2.07	2.28	3.32
WA-5	325	16.5	2.21E+10	0.92	44.37	0.0	8.02	2.35	2.81	3.95
WA-6	489	2.8	2.05E+09	0.58	1.95	0.0	2.88	1.03	1.07	1.57
WA-7	411	10.1	1.20E+10	0.53	5.67	0.0	8.47	2.18	3.14	4.61
WA-8	279	57.4	6.55E+10	0.68	9.08	0.0	8.23	2.72	3.07	4.51
WA-9[a]	278	6.0	5.31E+09	0.82	16.03	0.0	7.83	2.53	2.85	4.11
WA-10	271	8.6	8.34E+09	0.82	14.39	0.0	6.70	2.73	2.43	3.51
WA-11[a]	291	7.7	7.76E+09	0.85	20.44	0.0	5.98	2.07	2.22	3.26
WA-12	329	142.3	2.24E+11	0.92	37.78	0.0	6.04	2.08	2.18	3.12
WA-13	520	141.0	2.18E+11	0.27	0.50	0.0	8.09	2.54	2.85	4.03
WA-14	515	14.2	2.51E+10	0.97	85.90	0.0	5.49	3.01	1.95	2.76
WA-15	482	67.6	8.25E+10	0.95	29.83	0.0	3.27	1.65	1.16	1.66
WA-16	612	19.4	2.54E+10	0.89	21.01	0.0	5.21	2.79	1.88	2.70
WA-17	259	8.3	9.04E+09	0.92	29.40	0.0	5.27	2.18	1.85	2.60

[a] Used relationship Na* = 0.5*Si to correct for additions from hot springs, evaporites, borates and other non silicate Na sources.
[b] Ca/Na ratio of 0.70 used after Singh et al. (2005).

Table 4
Chemical weathering fluxes from the eastern syntaxis and other world rivers

Catchment	TDS flux	Silicate cation flux	CO$_2$ consumption by silicate weathering	Total SiO$_2$ flux
	Tons km^{-2} yr^{-1}		10^5 mol km^{-2} yr^{-1}	
Brahmaputra				
Po Tsangpo	41.3	2.5	0.9	0.40
L. Yarlung Tsangpo at Pai (Tibet)	22.2	0.5	0.2	0.15
Po Tsangpo and Yarlung Tsangpo	24.3	0.7	0.2	0.18
Syntaxis (Pasighat − Po + Pai)	526	34.2	15.2	8.6
Brahmaputra at Pasighat[a]	66	3.5	1.5	0.90
Brahmaputra at Chilmari[a,b]	113	6.9	3.0	1.60
Other world rivers[c]				
Amazon	25	2.2	0.5	1.2
Congo-Zaire	6	0.8	0.5	0.5
Ganga	42	7.9	4.5	0.6
Indus	18	1.8	0.6	0.2
Mekong	91	6.2	2.5	1.0
Mississippi	24	1.7	0.7	0.2

[a] Chemistry data from Singh et al. (2005); discharge from this study; Ca/Na of 0.7 and Mg/Na of 0.3 from Singh et al. (2005).
[b] Chemistry data for Gowahati used for flux calculations; Ca/Na and Mg/Na ratios from this study.
[c] Chemical flux data from Gaillardet et al. (1999) and references therein.

2005), which may explain high Cl$^-$ or SO$_4^{2-}$ concentrations in some samples within this area (05-Tibet-67 and 69) (Fig. 3). However, the location of most hot/warm springs along the Yarlung Tsangpo are poorly constrained, making it difficult to directly attribute high solute concentrations to the presence of any specific hydrothermal system.

Since many of the streams sampled have no detectable Cl$^-$ and catchments with high dissolved Cl$^-$ are often located adjacent to catchments which display no detectable Cl$^-$, we assume all chlorine inputs above rain water additions to be the result of Cl$^-$-rich hot springs or the weathering of evaporite salts, and correct stream solute concentrations for these additions. Measured ion concentra-

tions are corrected by multiplying the molar ion/Cl$^-$ ratio in local hot spring waters (Ping et al., 2000) by the molar concentration of Cl$^-$ in solution after correction for rainwater additions (Table 2; Ping et al., 2000).

In the Yarlung Tsangpo basin, there can be non-silicate sources of Na$^+$, such as sodium carbonate or borax (Pascoe, 1963). In basins with these types of Na$^+$ sources, correcting the dissolved Na$^+$ concentration based on Cl$^-$ concentrations will result in an overestimation of the amount of Na$^+$ derived from the weathering of silicate minerals. To correct for the addition of all types of non-silicate Na$^+$, we examine the relative molar proportions of rain water and hot spring corrected Na$^+$ and Si in our stream samples after Singh
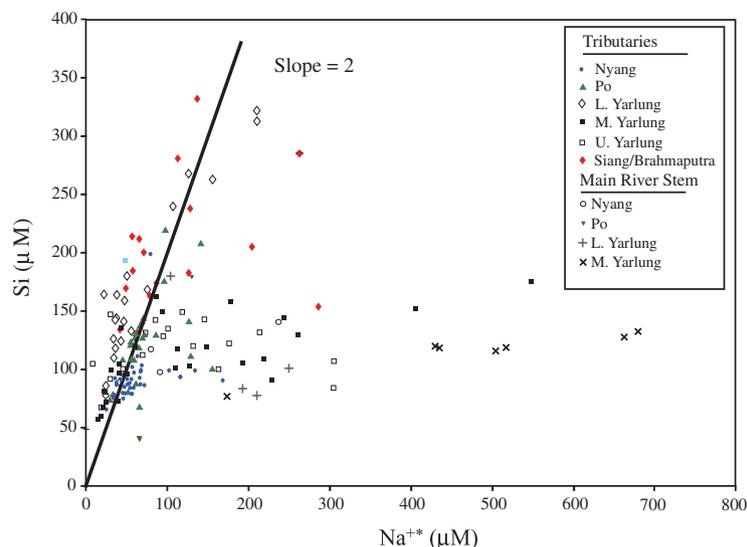
Fig. 6. Plot of the atmospheric and hot springs corrected Na^{+}* values against dissolved Si concentrations. Most samples fall about a line with a slope of 2, which reflects the expected relationship between Na$^+$ and Si for the weathering of plagioclase to kaolinite. Waters that fall off this line are corrected for the addition of non-silicate Na$^+$ based on the expected relationship shown here. Samples corrected in this manner are marked with an asterisk in Tables 1 and 2.

et al. (2005). A plot of corrected Na^{+*} versus dissolved Si (μM) concentrations shows that most samples fall about a line close to a slope of 2 (Fig. 6). This slope is close to the expected relationship for weathering of Na-silicates to kaolinite (Drever, 1997) and similar to the relationship between Si and Na^+ observed in the lower Tsangpo–Brahmaputra by Singh et al. (2005). Although the presence of kaolinite is typically indicative of deep weathering environments and might not be expected to form in the cold continental climate of the southern Tibetan plateau, the clay mineralogy of soils across an elevational gradient from 3700 to >4600 m in the Yarlung Tsangpo valley is dominated by micas, kaolinite, and lesser quantities of vermiculite (Smith et al., 1999). In addition, kaolinite comprises up to 50 wt% of the total clay fraction in some sediments in the distal Bengal fan (Brass and Raman, 1990). As a result, we corrected Na^+ concentrations in samples that fall well off the expected Na^+/Si relationship (Fig. 6), based on the expected relationship for the weathering of Na-silicates to kaolinite, which releases Na^+ and H_4SiO_2 in a Na^+/SiO_2 ratio of 0.5. To quantify the addition of excess Na^+ from non-silicate sources, we use this relationship for the weathering of sodium silicate to kaolinite (Singh et al., 2005). The Na_{excess}, which is defined here as $Na_{excess} = Na^* - Na^*_{Corrected}$ (where Na^* is the concentration of Na^+ in solution after correction for atmospheric and hot spring inputs and $Na^*_{Corrected}$ is the expected concentration of Na^+ in solution based on the expected relationship between Na^+ and Si for plagioclase weathering and kaolinite production) shows that in the main stem of the middle Yarlung Tsangpo, greater than 50% of dissolved Na^+ may be derived from the weathering of non-silicate, non-sodium chloride sources such as borates (Pascoe, 1963). In addition,

many of these streams that are characterized by a sodium excess are also characterized by high SO_4^{2-} concentrations and elevated SO_4^{2-}/Ca^{2+} ratios. Streams with a Na_{excess} and SO_4^{2-}/Ca^{2+} ratios of >0.5 also exhibit high Cl^- concentrations. In these systems, Cl^- and SO_4^{2-} display a good correlation (Fig. 7), which indicates that the weathering of evaporites, including Ca-sulfates and other Na^+ sources such as Na-carbonate or borate, may be significant in these drainages.

5.4. Silicate versus carbonate weathering reactions

To first order, the composition of the bedrock underlying a basin is the dominant control of stream chemistry. As a result, variations in bulk rock composition or the presence of trace quantities of highly weatherable rocks or minerals in a catchment can generate significant differences in dissolved chemical components. The basins examined in this study are primarily underlain by rocks of four major compositions: (1) granite/granitic gneiss, (2) schist/other felsic volcanic, (3) mafic volcanics, and (4) sedimentary and metamorphosed sedimentary units including silt-, clay- and sandstone units (Appendix A). However, because the majority of streams are characterized by dominantly felsic materials (>90% on average) in the bedload, many streams have similar dissolved Si chemistry and most dissolved Si concentrations are between 75 and 150 μmol L^{-1}. Major cation concentrations are more variable in stream samples than dissolved Si concentrations, and results from the fact that unlike Si, the dissolved concentration of other ions such as Ca^{2+}, Mg^{2+} and Na^+ is readily influenced by the presence of trace amounts of carbonates or evaporites within a basin. When even trace amounts of these rock types are present, the overall stream chemistry may be dominated by the weathering of these rocks. This may be the case in the Siang, where Ca^{2+} concentrations are extremely high, likely owing to the weathering of carbonate-rich sedimentary units or Ca-rich mafic rocks.

In many weathering environments, the chemical weathering of silicate minerals results in the formation of secondary clays. Although the clay content of the bedload of the Brahmaputra is relatively low, comprising only 2–3% of total sediments (Singh et al., 2005), illite, kaolinite, and chlorite (Sarin et al., 1989; Brass and Raman, 1990) are all found within the clay-sized fraction of Brahmaputra sediments. To understand the dominant chemical weathering processes in the Tsangpo–Brahmaputra in Tibet, we consider here the weathering of plagioclase, biotite and potassium feldspar to kaolinite and smectite as well as the weathering of biotite to vermiculite after the method described in Jacobson et al. (2003).

Ternary diagrams can provide a useful tool for understanding the primary chemical weathering reactions in a system. By plotting the composition of stream waters with respect to important chemical components we can evaluate the weathering reactions occurring in a drainage basin. For example, when plagioclase chemically weathers it can result in the production of kaolinite. This releases Na^+ and H_4SiO_2 into solution in a ratio of 0.5 (Drever, 1997). When plagioclase weathers to form smectite and other secondary products, the molar ratio of Na^+/SiO_2 released in this pro-

Fig. 7. Cl^- concentrations against SO_4^{2-} concentrations for streams from the middle and upper Yarlung Tsangpo that are characterized by Na-excess (marked by an asterisk in Table 1) and less than 1000 μM SO_4^{2-}. The relationship between Cl^- and SO_4^{2-} shown here indicates inputs from the weathering of evaporite minerals in some stream systems in the arid portions of the Yarlung Tsangpo catchment.

cess is dependent upon the Ca^{2+}/Na^+ ratio of the plagioclase. We used microprobe analyses from 42 plagioclase grains from granitic rocks along the Yarlung Tsangpo, Namche Barwa syntaxis, and Po Tsangpo to calculate an average plagioclase Ca^{2+}/Na^+ ratio of 0.545 (A. Booth, personal communication) and assumed secondary smectites to have an average layer charge of 0.33 (Moore and Reynolds, 1997). Thus, the weathering of plagioclase and production of Ca-beidellite would release a molar Na^+/SiO_2 ratio of 1.25. The weathering of plagioclase and production of Na-beidellite would release a molar Na^+/SiO_2 ratio of 0.88 (Drever, 1997). A plot of the relative molar proportions of Ca^{2+}, Na^+, and dissolved Si shows that nearly all stream waters fall along a mixing line defined by calcite weathering and kaolinite production (Fig. 8). Some samples fall off this line, and instead may plot along a mixing line defined by the production of smectite and the weathering of calcite.

To examine whether biotite weathering and vermiculite production is significant, we also examined reactions involving the release of K^+. Biotite and potassium feldspar are the dominant source of K^+ in the study area and weathering reactions involving these minerals would be expected to release K^+ to solution. A plot of the relative molar proportion of Na^+, dissolved Si, and K^+ in stream waters shows that most samples fall in a broad pattern around a mixing line defined by the weathering of plagioclase to kaolinite and the weathering of biotite to vermiculite (Fig. 9). Some samples, particularly main stem river samples and waters from tributaries of the middle and upper Yarlung Tsangpo, fall off this mixing line, trending toward inputs of dissolved Na^+. These may reflect weathering of evaporites, Na-carbonates, or borates within some of the arid western basins (Pascoe, 1963).

Despite relatively few carbonate rocks identified in the stream bedload of any drainages sampled, the solute chemistry of nearly all stream waters examined is strongly influenced by carbonate weathering reactions, with most streams displaying high dissolved Ca^{2+} and HCO_3^- and relatively high Mg^{2+}/Ca^{2+} ratios (Figs. 4 and 5). In light of the potential for significant Ca^{2+} fluxes from the weathering of small amounts of calcite in a drainage, it is important to be able to distinguish between carbonate and silicate sources of Ca^{2+} and Mg^{2+}. This is particularly important because only the weathering of silicate minerals can result in the net consumption of atmospheric CO_2 via the weathering process. Studies from tributaries of the lower Brahmaputra and Ganges show that Ca^{2+} and Mg^{2+} account for more than 80% of dissolved cations in highland rivers (Sarin et al., 1989) and in the headwaters of the Ganga (Krishnaswami et al., 1998). In the lower Brahmaputra, up to 75% of all cations may be derived from carbonate weathering (Singh et al., 2005). To determine the relative role of carbonate and silicate weathering on the release of Ca^{2+} and Mg^{2+} in the major tributaries of the Tsangpo–Brahmaputra, we calculated the carbonate weathering index (CWI) after Harris et al. (1998). Basins in which carbonate weathering provides the majority of the total dissolved Ca^{2+} and Mg^{2+} species will have high a CWI index (>0.5) while catchments with less significant inputs by carbonate weathering are expected to display a low (<0.5) CWI index. The carbonate weathering index (CWI) is defined as:

$$CWI = \left[\left(\frac{Ca}{Na^*} \right) + \left(\frac{Mg}{Na^*} \right) - \alpha \right] \Big/ \left[\left(\frac{Ca}{Na^*} \right) + \left(\frac{Mg}{Na^*} \right) \right]$$

where $\alpha = (Ca/Na)_{Plagioclase} + (Mg/Na)_{Rock}$.

The Ca/Na ratio used here (0.545) is taken from electron microprobe measures of 42 plagioclase grains from samples collected along the Yarlung Tsangpo, Po Tsangpo, and Namche Barwa area (Booth et al., 2004) and is the same
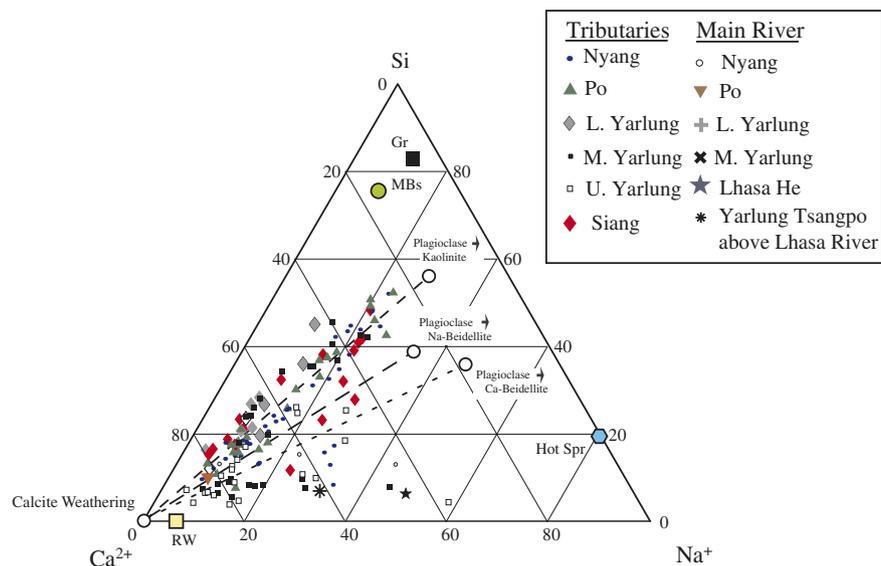
Fig. 8. Ternary diagram of the dissolved Ca^{2+}, Na^+ and dissolved Si concentration of stream waters. Most samples fall along a mixing line defined by the release of Ca^{2+} during calcite weathering and the production of kaolinite during the weathering of plagioclase. Samples that fall off this line likely reflect additions from hot springs or evaporite weathering in the basin. The bulk composition of rainwater (RW), hot springs (Hot Spr), calcite, granite (Gr), and metabasalts (MBs) are shown.
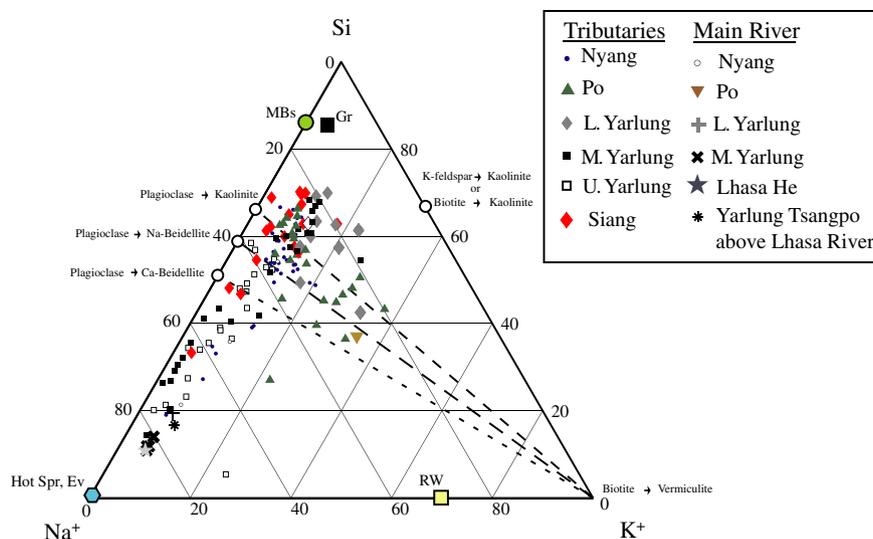
Fig. 9. Ternary diagram of the dissolved Na^+, K^+ and SiO_2 concentration of stream waters. Most samples fall in an array along the mixing line defined by the release of K^+ during biotite weathering and vermiculite production and the weathering of plagioclase to kaolinite. A number of samples highlight weathering processes that release Na^+ to solution, particularly waters in the western, arid portions of the Yarlung basin. The bulk composition of rainwater (RW), hot springs (Hot Spr), evaporites (Ev), calcite, granite (Gr), and metabasalts (MBs) are shown.

value used to define weathering reaction mixing lines in Figs. 8 and 9. This value rests between the values of 0.2 and 0.7 used in previous studies of the Brahmaputra to estimate the percentage of ions derived from carbonate weathering (Galy and France-Lanord, 1999; Jacobson et al., 2002; Singh et al., 2005). Based on major element chemistry of southeastern Tibetan granitoids (Booth et al., 2004) we use a Mg^{2+}/Na^+ ratio of bulk silicate rocks of 0.30, which is similar to calculated values in Galy and France-Lanord (1999) and the value reported in Krishnaswami et al. (1999). It is important to note however, that the Ca^{2+}/Na^+ and Mg^{2+}/Na^+ ratio used to calculate the relative proportion of Ca^{2+} and Mg^{2+} ions derived from carbonate or silicate weathering can impart a significant degree of error on these estimates, particularly in basins that are not large enough to average the chemical heterogeneity of bedrock formations. This could have the effect of generating over- or under-estimates of the amount of Ca^{2+} and Mg^{2+} ions derived from carbonate weathering. Furthermore, contributions of Ca^{2+} from the weathering of evaporites such as gypsum or anhydrite may also generate overestimates of the degree of carbonate weathering. However, studies of southern Tibetan hot springs (Ping et al., 2000) suggest that sulfate-rich hydrothermal waters are generated from pyrite oxidation rather than gypsum weathering which would limit non-silicate, non-carbonate, Ca^{2+} sources. In addition, studied basins are generally of similar enough composition that they fit the chemical stoichiometry used here. As a result, the CWI is a reasonable approximation of the importance of carbonate weathering in our study areas.

The calculated carbonate weathering index (CWI) ranges from 0.26 to 0.98 for all streams analyzed and is shown in Table 2. Most streams in the area immediately upstream of Namche Barwa have CWI values close to 0.9 and samples from tributaries of the middle and upper Yarlung Tsangpo

exhibit similar CWI values (Table 2). Samples south of the syntaxis along the Siang also show similarly high CWI values, which are consistent with streams draining carbonate-rich sedimentary units. These data indicate that the Ca^{2+} and Mg^{2+} fluxes in rapidly uplifting portions of the syntaxis and the western portion of our study area are dominated by carbonate weathering reactions, despite the fact that we observed very little carbonate rocks in these drainages.

One potential source of this carbonate is calcite veins within schists and other felsic volcanics or in shallow hydrothermal systems. These types of calcite vein systems have been identified in other tectonically active areas (Koons et al., 1998; Chamberlain et al., 2002; Jacobson et al., 2002) and are thought to form through the development of hydrothermal vein systems. Because calcite dissolution rates are several orders of magnitude faster than plagioclase (Chou et al., 1989; Blum and Stillings, 1995), even small quantities of calcite in veins can exert significant control on Ca^{2+} and Sr^{2+} fluxes (Blum et al., 1998; Chamberlain et al., 2005). As a result, vein calcite may be an important contributor to cation budgets in Yarlung Tsangpo. However, Mg^{2+}/Ca^{2+} ratios are relatively high, suggesting there could be loss of Ca^{2+} from the system through secondary calcite precipitation or possibly a high-Mg carbonate source such as dolomite that is destroyed in transport and thus absent from the stream bedload. One means of evaluating whether secondary calcite precipitation can influence Mg^{2+}/Ca^{2+} ratios is by examining the calcite or dolomite saturation index of a stream. Using stream temperature, pH, and solute chemistry, we calculated whether or not each stream system was saturated with respect to calcite or dolomite using Geochemist's workbench (Bethke, 1996). A plot of the mineral saturation index (Fig. 10) shows that in general, most streams are undersaturated with respect to these minerals. However, a number of tributaries in the middle and upper Yarlung basin
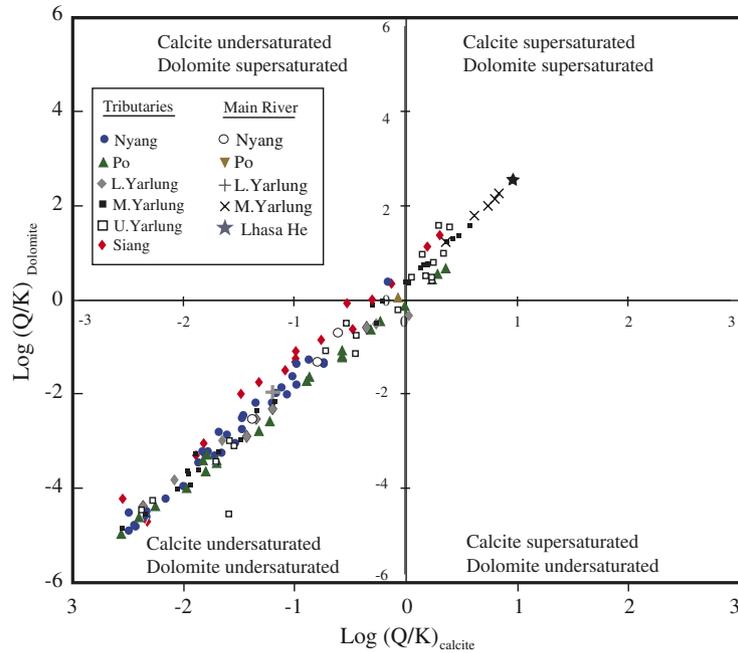
Fig. 10. Calcite and dolomite saturation indices for all stream waters analyzed. The plot of saturation indices for stream waters show that most streams are undersaturated with respect to calcite and dolomite. A number of streams in the far western portions of the study area and in the immediate vicinity of the eastern syntaxis show both calcite and dolomite supersaturation.

and from the most rapidly uplifting portion of the study area in the Po and lower Yarlung basins adjacent to the Namche Barwa syntaxis, are close to or supersaturated with respect to calcite and dolomite. In these streams, supersaturation of carbonate species may result in the preferential precipitation of secondary calcite during fluvial transport. In some Himalayan waters (Jacobson et al., 2002; Bickle et al., 2005), up to ~70% of Ca^{2+} derived from carbonate weathering may be removed during transport from the High Himalaya to Lesser Himalaya due to changes in stream temperature and degassing of CO_2 from stream waters resulting in an increase in Mg^{2+}/Ca^{2+} ratios. Thus, Ca^{2+}/Na^+ or Mg^{2+}/Na^+ ratios in solution may change during transport of solutes. If vein calcite is the main source of carbonate in the Yarlung Tsangpo upstream of the syntaxis, this process may help account for the high Mg^{2+}/Ca^{2+} ratios observed in these stream waters.

5.5. Chemical denudation rates in the Yarlung Tsangpo–Brahmaputra basin

To determine the effects of factors such as climate and tectonics on chemical denudation rates, it is necessary to quantify the total flux generated from the weathering of silicate and carbonate rocks. To calculate the total chemical weathering rates of carbonates (CRW_{carb}) and silicates (CWR_{sil}) we use average plagioclase Ca^{2+}/Na^+ ratios, average bulk rock Mg^{2+}/Na^+, corrected K^+, Ca^{2+}, and Na^* or $Na^*_{Corrected}$ concentrations and assume all non-silicate, non-hydrothermal Ca^{2+} and Mg^{2+} to be of carbonate origin. It is important to note however, that for some of the streams in the upper Yarlung Tsangpo that may receive additions of Ca^{2+} from gypsum weathering, this assumption could result in an overestimation of the CWR_{Carb}. We calculated the

total flux of cations derived from the weathering of carbonate and silicate components according to the methods outlined in Mortatti and Probst (2004) and Galy and France-Lanord (1999) and modified here to include hot spring/evaporite inputs. The amount of Ca^{2+} derived from silicates and carbonates can be approximated by:

$$Ca^{2+}_{Sil} = (Ca/Na)_{Plagioclase} \times Na^* \text{ and}$$
$$Ca^{2+}_{Total} = Ca^{2+}_{Carb} + Ca^{2+}_{Sil} + Ca^{2+}_{Hot\ springs}$$

Because hot springs are not a significant source of Mg^{2+}, the molar quantity of Mg-derived from the weathering of silicates can be similarly approximated by:

$$Mg_{Sil} = (Mg/Na)_{Rock} \times Na^*$$
$$Mg^{2+}_{Total} = Mg^{2+}_{Carb} + Mg^{2+}_{Sil}$$

From these the chemical weathering rate of carbonates and silicates are approximated by the total mass flux of cations from each component:

$$CWR_{Carb} = Ca^{2+}_{Carb} + Mg^{2+}_{Carb}$$
$$CWR_{Sil} = K^+_{Sil} + Na^{+*} + Ca^{2+}_{Sil} + Mg^{2+}_{Sil}$$
$$CWR_{Hot\ springs} = K^+_{Hot\ springs} + Ca^{2+}_{Hot\ springs} + Na^+_{Hot\ springs}$$

In this calculation, the component of each ion derived from hot springs depends on the ion/Cl^- ratio and the concentration of Cl^- in solution after correction for rain water additions and:

$$K^+_{Hot\ springs} = 0.09 \times Cl^-$$
$$Ca^{2+}_{Hot\ springs} = 0.01 \times Cl^-$$
$$Na^+_{Hot\ springs} = 0.73 \times Cl^-$$

Total CO_2 consumption by silicate weathering can be approximated by the total molar charge equivalents of all cations generated by silicate weathering. This can be calculated by the following formula:

$$F_{CO_2} = 2 \times Ca^{2+}{}_{Sil} + 2 \times Mg^{2+}{}_{Sil} + K^+{}_{Sil} + Na^*$$

In this equation, factors of 1 are applied to K^+ and Na* and 2 for Ca^{2+} and Mg^{2+}, for the stoichiometric coefficients of weathering reactions for cations released and alkalinity produced by weathering reactions (Mortatti and Probst, 2004).

CWR_{carb} and CWR_{sil} for the tributaries along the Nyang, Po, Yarlung Tsangpo, Lhasa He, and Siang vary significantly in response to tectonic and climatic factors. In tributaries along the Nyang, the CWR_{carb} rates are relatively low, between 0.16 and 3 tons km^{-2} yr^{-1}, although two of the high elevation streams (05-Tibet-1 and 05-Tibet-2) exhibit CWR_{Carb} up to 9 tons km^{-2} yr^{-1}. In general, streams in this drainage system are well below measures for the bulk Ganga–Brahmaputra ($\sim$34 tons km^{-2} yr^{-1}). Likewise, CWR_{sil} for these tributaries are also low, and range from 0.30 to 1.25 tons km^{-2} yr^{-1}. Streams draining into the middle Yarlung Tsangpo show similarly low rates of CWR_{sil}, however CWR_{carb} are nearly an order of magnitude higher ($\sim$21 tons km^{-2} yr^{-1}) in a number of these drainages, and are characterized by high Cl^- concentrations and excess Na^+ (05-Tibet-90–05-Tibet-103). These apparently high carbonate weathering rates could reflect evaporite weathering in these basins, as these drainages are also characterized by elevated Ca^{2+}, SO_4^{2-}, and Cl^- concentrations. If all SO_4^{2-} in these streams were derived from the weathering of gypsum, calculated CWR_{Carb} rates for these streams would be similar to the low CWR_{Carb} observed in the Nyang and Po drainages. However, dissolved SO_4^{2-} in these drainages generally exceeds the Ca^{2+} concentration, which suggests that sulfide oxidation in hot springs may also be a significant source of SO_4^{2-}. In the upper Yarlung, CWR_{carb} are similarly high, ranging from $\sim$1 to 13 tons km^{-2} yr^{-1} and the CWR_{Sil} is generally <1 tons km^{-2} yr^{-1}. These data show that across much of the southern Tibetan plateau, chemical denudation rates are low and reflect the relatively low rates of precipitation and erosion in the middle and upper portions of the Yarlung Tsangpo. In contrast, streams in the Po Tsangpo basin and along the lower Yarlung Tsangpo near the Namche Barwa syntaxis show consistently higher CWR_{carb} and CWR_{sil} than western basins. In the Po Tsangpo, CWR_{carb} values range from 0.3 to 18.6 tons km^{-2} yr^{-1} and CWR_{sil} from 0.5 to 5.4 tons km^{-2} yr^{-1}. In tributaries closest to Namche Barwa, CWR_{carb} values range from 1.1 to 32.1 tons km^{-2} yr^{-1} and CWR_{sil} from 0.5 to 12.4 tons km^{-2} yr^{-1}. Some of the highest values are located in the area closest to the syntaxis and the areas of the most rapid exhumation (Fig. 2; Table 2). The highest CWR_{sil} in these areas are more than an order of magnitude greater than rates in streams draining into the upper and middle Tsangpo. However, tributaries of the Siang show consistently high CWR_{Carb} due to the high abundance of carbonate-bearing rocks south of the eastern syntaxis and high CWR_{Sil} due to high precipitation. These data support weathering models that show that rapid rates of chemical weathering are generated in areas of rapid surface uplift or erosion (Riebe et al.,

2001; Riebe et al., 2004; Chamberlain et al., 2005; Waldbauer and Chamberlain, 2005).

Rapid chemical denudation in the eastern syntaxis generates markedly higher rates of CO_2 consumption by silicate weathering than in areas with lower rates of uplift. In this area, CO_2 consumption by silicate weathering is nearly an order of magnitude greater than other portions of the Yarlung Tsangpo–Brahmaputra in Tibet, and reaches $\sim$5.5 $\times$ 10^5 mol km^{-2} yr^{-1} in streams east of Pai. However, the high concentrations of SO_4^{2-} in many tributaries suggest that part of the silicates may be weathered by H_2SO_4 generated during pyrite oxidation. As a result, these estimates of CO_2 consumption by silicate weathering may be an upper estimate.

In general, the total flux of cations derived from hot springs is less than 1–2% of the total cation flux, however it may exceed 15% in some streams in the middle Yarlung Tsangpo. These streams, such as 05-Tibet-100 and W-2-7, are characterized by extremely high dissolved Cl^- concentrations of up to 440 μM as well as elevated Na^+ concentrations. The large inputs from hot springs or sodium chloride evaporites in these stream samples are evidenced in the ternary diagrams shown in Figs. 8 and 9.

5.6. Relationships between climate, tectonics, and chemical weathering

The Tsangpo–Brahmaputra spans a wide range of climatic and tectonic environments. As a result, chemical weathering rates may be expected to vary dramatically across the study area in response to changes in climatic, tectonic, or geomorphic factors (Millot et al., 2002; West et al., 2005). Because major ions such as Ca^{2+} and Mg^{2+} may be easily influenced by the weathering of trace carbonates and Na^+ is affected by hydrothermal inputs and evaporite weathering, dissolved Si fluxes may provide a good measure of overall silicate weathering rates. We use it here as a means of examining the role of climatic and geomorphic factors on silicate weathering. In contrast to previous studies of climate and weathering (White and Blum, 1995; Dalai et al., 2002) dissolved Si and base cation concentrations show little or no correlation with the stream temperature at the time of sampling. This is likely due to the relatively narrow range of temperatures observed during our sampling period and the larger influences of changing geologic and geomorphic conditions. However, precipitation or runoff is shown to be one of the primary controls of chemical weathering rates on a global scale (Bluth and Kump, 1994; White and Blum, 1995; Gaillardet et al., 1999). Stream chemistry and weathering flux data from the Tsangpo support this, and show a strong correlation between dissolved Si fluxes and precipitation (Fig. 11). This relationship could be expected since annual fluxes for the streams studied are calculated using TRMM satellite precipitation data. However, the relationship between dissolved Si fluxes and precipitation is in good agreement with previous studies of humid tropical watersheds (Oliva et al., 2003). These data do, however, have a steeper slope than that observed by White and Blum (1995) in their analysis of global silicate weathering
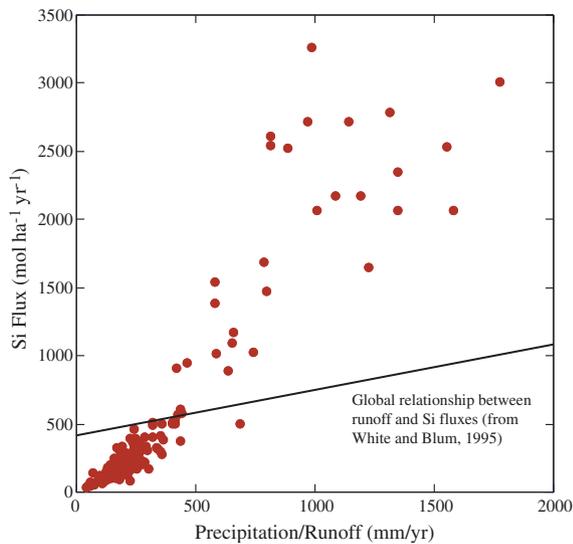
Fig. 11. Plot of precipitation/runoff versus measured Si flux (mol ha^{-1} yr^{-1}) for Yarlung Tsangpo. Si fluxes exhibit a strong correlation with precipitation/runoff with a slope similar to that observed in tropical humid watersheds. Solid black line represents the slope of the relationship between Si and runoff for a global data set (White and Blum, 1995).

fluxes and precipitation/runoff. As a result, in the Yarlung Tsangpo, high precipitation/runoff generates higher dissolved Si fluxes than would be predicted from the relationship between precipitation/runoff and Si fluxes observed in a global dataset (White and Blum, 1995). This may be due in part to the relatively high rates of tectonic uplift in the eastern Himalayan region where the precipitation is the highest, as well as the influence of recent glaciations which provide large volumes of easily weathered fine materials.

Although there are few erosion rate measurements along the Yarlung Tsangpo and in the eastern syntaxis, one means of examining the relationship between erosion and chemical weathering fluxes is to look at spatial variability of weathering. A plot of the calculated annual dissolved Si and CWR$_{Sil}$ flux against the longitudinal profile of the Tsangpo and calculated stream power shows that dissolved Si fluxes are high in sections of the Brahmaputra drainage characterized by a relatively steep river profile and high stream power (Fig. 12). These steep sloped, highly erosive regions may continually expose fresh rock to weathering through landsliding, glaciation, or river incision and combined with high precipitation, may result in extremely high weathering fluxes. This is particularly well evidenced in the region ~1500–1700 km downstream of the river headwaters and in the eastern syntaxis region (~2000 km downstream) where dissolved Si fluxes closely mirror measured stream power. These data suggest that in this system, climatic and tectonic factors that result in high rates of physical erosion also generate high rates of chemical weathering and attests to the strong links between climatic, tectonic, and geomorphic factors and chemical weathering.

5.7. The role of the eastern syntaxis of the Himalaya on the chemical weathering budget of the Brahmaputra

Quantifying chemical weathering fluxes in the eastern syntaxis of the Himalaya is important because rapid rock uplift and heavy monsoonal precipitation in this area may have resulted in high rates of silicate weathering and CO$_2$ consumption over millions of years. To quantify these fluxes, we examined the difference in chemical weathering fluxes in the Brahmaputra below the eastern syntaxis at Pasighat (Singh et al., 2005) and the combined flux in the Yarlung Tsangpo at Pai and the Po Tsangpo upstream of Gyala Peri. One recent estimate of CO$_2$ consumption from the syntaxis uses this approach based on a water sample from the Brahmaputra at Pai and one at Pasighat (Singh et al., 2005). We apply the same approach here, adding river data from the Po Tsangpo, north of Namche Barwa. Based on river chemistry, average Ca/Na$_{Plagioclase}$ and Mg/Na$_{Rock}$ values, and current estimates of the river discharge, we show that the annual flux of TDS (tons km^{-2} yr^{-1}) from the Po Tsangpo is nearly twice that of the lower Yarlung Tsangpo at Pai. Similarly, the silicate cation flux and CO$_2$ consumption by weathering are both four to five times greater in the Po than the Yarlung Tsangpo at Pai. In total, the TDS flux from the eastern syntaxis is greater than 526 tons km^{-2} yr^{-1} and CO$_2$ consumption by silicate weathering is 15.2×10^5 mol km^{-2} yr^{-1} which is more than twice the Brahmaputra average and forty times greater than the CO$_2$ consumption rates for the Tibetan portion of the drainage. This represents more than 15% of the Brahmaputra total from only 4% of the total basin drainage area. If the total CO$_2$ consumption by weathering is approximated by the total SiO$_2$ flux (8.6×10^5 mol km^{-2} yr^{-1}) where 1 mol Si equals 2 mol CO$_2$ consumed (Edmond and Huh, 1997), weathering in the syntaxis would be expected to account for more than 20% of the total CO$_2$ consumption in the Brahmaputra. While measures of TDS in the syntaxis are higher than previous measures, our calculation of total CO$_2$ consumption by silicate weathering in the eastern syntaxis is less than that of Singh et al. (2005). This is due to differences in elemental concentrations at the time of sampling, estimates of stream discharge at Pai and Pasighat, and differences in the Ca^{2+}/Na$^+$ and Mg^{2+}/Na$^+$ ratios used to calculate silicate versus carbonate flux components. Additionally, our calculation is lower because we include stream data from the Po Tsangpo, which is a drainage that shows relatively high chemical weathering fluxes. However, our calculations support previous studies that show that the eastern syntaxis has a significant impact on the chemical fluxes in the Brahmaputra (Singh et al., 2005) and dominates sediment fluxes (Singh and France-Lanord, 2002).

While chemical weathering in the syntaxis dominates the riverine chemical load of the Brahmaputra, recent studies (Moore, 1997; Dowling et al., 2003) suggest that chemical weathering of sediments in the lower plains of the Ganga–Brahmaputra basin and the Bengal delta may generate a significant subsurface chemical flux (Dowling et al., 2003). Thus, the true impact of the rapid uplift and erosion of the
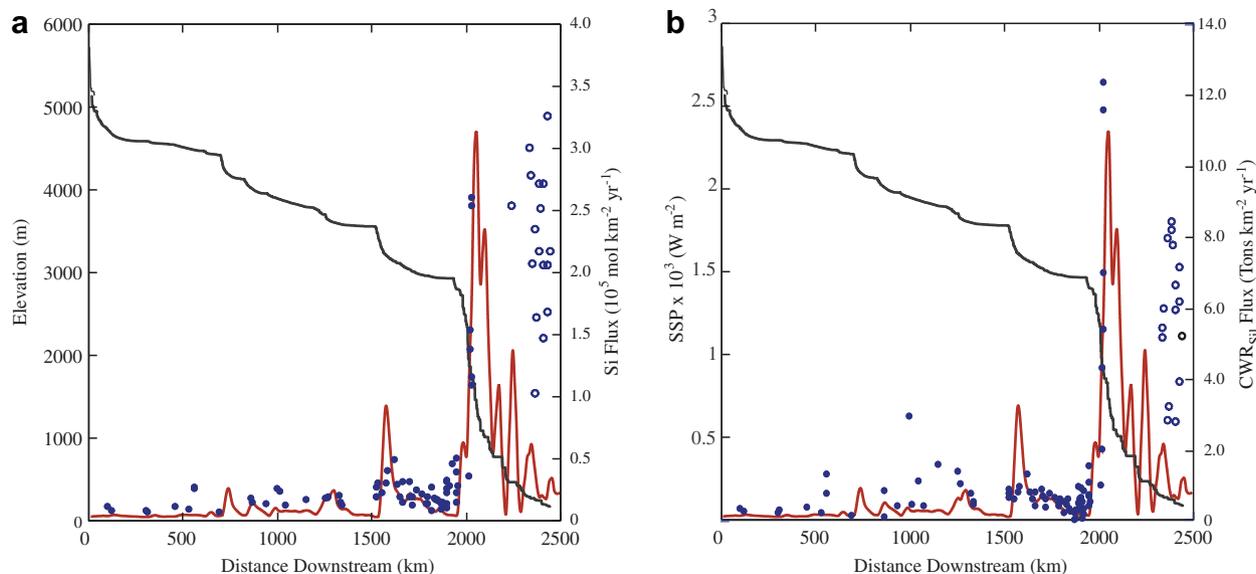
Fig. 12. (a) Plot of the measured Si flux (black circles; 10^5 mol km^{-2} yr^{-1}) against the longitudinal profile of the Yarlung Tsangpo–Brahmaputra (solid black line) overlain on measures of stream power (light grey line; 10^3 W m^{-2}). Si fluxes are highest in regions characterized by steep channel slope and high stream power and reach a maximum in the eastern syntaxis region. Si flux data from the Siang–Brahmaputra based on February stream chemistry is shown in open circles. (b) Measured CWR_{Sil} (black circles; tons km^{-2} yr^{-1}) against longitudinal profile and stream power (light grey line; 10^3 W m^{-2}). Flux data from the Siang–Brahmaputra is shown in open circles.

eastern syntaxis region on the chemical budget of the Ganges–Brahmaputra may be more significant than shown here, if the chemical flux from sediments generated in this area and weathered in the Bengal delta are included in total chemical weathering budgets.

6. CONCLUSIONS AND IMPLICATIONS

The examination of watershed geochemistry in the Tibetan tributaries of the Yarlung Tsangpo–Brahmaputra river attests to the strong links between tectonic and climatic processes and chemical weathering. Silicate weathering throughout most catchments in southern Tibet and in the eastern syntaxis of the Himalaya is dominated by the chemical breakdown of plagioclase and the production of kaolinite, however overall chemical weathering fluxes are strongly regulated by the dissolution of carbonate in the studied catchments. Roughly 80–90% of all Ca^{2+} and Mg^{2+} are derived from the weathering of these carbonates. This result supports previous studies (Blum et al., 1998; Jacobson et al., 2003) which demonstrate that in active tectonic environments, weathering fluxes are often dominated by carbonate weathering processes, even when there is little or no carbonate rock exposed within the catchment. Surprisingly however, hydrothermal inputs from the Himalayan geothermal belt and evaporite weathering in the arid western portion of the Yarlung basin provide significant inputs to many tributaries of the Tsangpo–Brahmaputra and may strongly affect solute budgets of these streams.

In total, chemical weathering in the Brahmaputra basin accounts for 2–3% of the total CO_2 consumption by silicate weathering world-wide (Singh et al., 2005). However, much of this weathering occurs in a relatively small area with extremely high rates of rock uplift and heavy monsoonal precipitation. Chemical weathering rates and CO_2 consumption by silicate weathering in the eastern syntaxis of the Himalaya are nearly an order of magnitude higher than the world average and are close to weathering rates for some of the most rapidly eroding basaltic terrains. Total CO_2 consumption by silicate weathering in this area accounts for more than 15–20% of the total in the Brahmaputra basin despite making up only 4% of the total basin area. High chemical fluxes in the eastern syntaxis are driven by rapid rock exhumation (3–10 mm yr^{-1}) and heavy monsoonal precipitation, which generates large volumes of sediment that are mobilized through frequent landslides and removed by fluvial processes. As a result, long-term changes in the rate of tectonic uplift in this area or the intensity of the monsoon over this region could have dramatic consequences for the weathering budget of one of the world's major rivers and for global CO_2 consumption by silicate weathering.

APPENDIX A

Sample	Granite/ granitic gnesiss (%)	Schist/other felsic volcanics (%)	Mafic volcanics (%)	Quartzite (%)	Conglomerate (%)	Other (%)
Nyang Tsangpo basin tributaries						
05Tibet-01	22	74	0	0	0	4
05Tibet-02	23	77	0	0	0	0
05Tibet-04	4	84	8	4	0	0
05Tibet-05	14	84	2	0	0	0
05Tibet-06	8	92	0	0	0	0
05Tibet-07	58	42	0	0	0	0
05Tibet-09	76	20	0	0	0	4
05Tibet-10	32	62	2	4	0	0
05Tibet-11	58	32	4	0	0	6
05Tibet-12	54	44	2	0	0	0
05Tibet-13	18	74	8	0	0	0
05Tibet-14	21	64	15	0	0	0
05Tibet-15	86	14	0	0	0	0
05Tibet-16	76	24	0	0	0	0
05Tibet-17	54	46	0	0	0	0
05Tibet-18	54	31	15	0	0	0
05Tibet-19	49	29	22	0	0	0
05Tibet-20	49	29	22	0	0	0
05Tibet-21	13	80	7	0	0	0
05Tibet-22	51	45	4	0	0	0
05Tibet-23	12	76	12	0	0	0
05Tibet-24	2	96	2	0	0	0
05Tibet-25	4	71	24	0	0	0
05Tibet-26	63	30	8	0	0	0
05Tibet-27	2	72	26	0	0	0
05Tibet-28	4	72	24	0	0	0
05Tibet-29	0	90	10	0	0	0
05Tibet-30	100	0	0	0	0	0
05Tibet-32	28	40	32	0	0	0
05Tibet-33	28	72	0	0	0	0
05Tibet-36	100	0	0	0	0	0
05Tibet-59	84	16	0	0	0	0
05Tibet-60	88	0	12	0	0	0
05Tibet-61	96	0	4	0	0	0
Nyang Tsangpo						
05Tibet-03	18	82	0	0	0	0
05Tibet-08	47	44	6	3	0	0
05Tibet-31	—	—	—	—	—	—
Po Tsangpo basin tributaries						
05Tibet-35	80	0	20	0	0	0
05Tibet-37	75	0	25	0	0	0
05Tibet-38	72	0	28	0	0	0
05Tibet-39	75	0	25	0	0	0
05Tibet-40	96	0	4	0	0	0
05Tibet-41	96	0	4	0	0	0
05Tibet-42	84	0	16	0	0	0
05Tibet-43	72	0	28	0	0	0
05Tibet-44	88	0	12	0	0	0
05Tibet-45	80	0	15	0	0	5
05Tibet-46	96	0	4	0	0	0
05Tibet-47	32	20	44	4	0	0
05Tibet-48	79	0	17	4	0	0
05Tibet-49	79	0	19	2	0	0
05Tibet-50	92	0	8	0	0	0
05Tibet-51	96	0	4	0	0	0
05Tibet-52	100	0	0	0	0	0
05Tibet-53	96	0	4	0	0	0

Appendix A (*continued*)

Sample	Granite/ granitic gnesiss (%)	Schist/other felsic volcanics (%)	Mafic volcanics (%)	Quartzite (%)	Conglomerate (%)	Other (%)
05Tibet-54	100	0	0	0	0	0
05Tibet-55	84	4	12	0	0	0
05Tibet-56	80	8	12	0	0	0
05Tibet-57	96	0	4	0	0	0
05Tibet-58	80	20	0	0	0	0
Po Tsangpo						
05Tibet-34	—	—	—	—	—	—
Lower Yarlung Tsangpo basin tributaries						
05Tibet-63	58	30	10	2	0	0
05Tibet-64	83	6	6	4	0	0
05Tibet-67	100	0	0	0	0	0
05Tibet-68	100	0	0	0	0	0
05Tibet-69	96	0	4	0	0	0
05Tibet-70	88	0	4	8	0	0
05Tibet-71	96	0	4	0	0	0
05Tibet-72	96	0	4	0	0	0
05Tibet-73	96	0	4	0	0	0
05Tibet-74	96	0	4	0	0	0
05Tibet-75	96	0	4	0	0	0
Lower Yarlung Tsangpo						
05Tibet-62	—	—	—	—	—	—
Middle Yarlung Tsangpo basin tributaries						
05Tibet-65	68	14	14	4	0	0
05Tibet-66	92	0	8	0	0	0
05Tibet-76	100	0	0	0	0	0
05Tibet-77	4	80	16	0	0	0
05Tibet-78	84	4	10	2	0	0
05Tibet-79	84	0	12	4	0	0
05Tibet-80	90	0	10	0	0	0
05Tibet-81	96	0	4	0	0	0
05Tibet-82	92	0	8	0	0	0
05Tibet-84	94	0	4	2	0	0
05Tibet-85	100	0	0	0	0	0
05Tibet-86	100	0	0	0	0	0
05Tibet-87	100	0	0	0	0	0
05Tibet-89	18	42	38	0	0	2
05Tibet-90	4	82	14	0	0	0
05Tibet-91	2	98	0	0	0	0
05Tibet-92	31	69	0	0	0	0
05Tibet-93	0	56	12	32	0	0
05Tibet-95	4	84	12	0	0	0
05Tibet-96	0	100	0	0	0	0
05Tibet-97	0	100	0	0	0	0
05Tibet-98	48	22	0	0	30	0
05Tibet-99	0	100	0	0	0	0
05Tibet-100	64	36	0	0	0	0
05Tibet-101	8	30	28	0	34	0
05Tibet-103	14	86	0	0	0	0
Middle Yarlung Tsangpo river						
05Tibet-83	100	0	0	0	0	0
05Tibet-88	100	0	0	0	0	0
05Tibet-94	—	—	—	—	—	—
05Tibet-102	—	—	—	—	—	—
05Tibet-104	—	—	—	—	—	—
05Tibet-105	—	—	—	—	—	—
05Tibet-106	—	—	—	—	—	—

REFERENCES

Anders A. M., Roe G. H., Hallet B., Montgomery D. R., Finnegan N. J., and Putkonen J. (2006) Spatial patterns of precipitation and topography in the Himalaya. In *Tectonics, Climate and Landscape Evolution.* GSA Special Paper, vol. 398 (eds. S. D. Willett, N. Hoovius, M. T. Brandon, and D. M. Fisher), pp. 39–53.

Berner E. K., and Berner R. A. (1996). *Global Environment: Water, Air, and Geochemical Cycles.* Prentice Hall, New Jersey.

Bethke C. M. (1996) *Geochemical Reaction Modeling: Concepts and Applications.* Oxford University Press, New York, 397 p.

Bickle M. J., Chapman H. J., Bunbury J., Harris N. B. W., Fairchild I. J., Ahmad T., and Pomies C. (2005) Relative contributions of silicate and carbonate rocks to riverine Sr fluxes in the headwaters of the Ganges. *Geochim. Cosmochim. Acta* **69**, 2221–2240.

Blum A. E., and Stillings L. L. (1995) Chemical weathering of feldspars. In *Chemical Weathering Rates of Silicate Minerals. Min. Soc. Am. Rev. Min.*, vol. 31 (A. F. White and S. L. Brantley), pp. 291–351.

Blum J. D., Gazis C. A., Jacobson A. D., and Chamberlain C. P. (1998) Carbonate versus silicate weathering in the Raikhot watershed within the high Himalayan crystalline series. *Geol.* **26**, 411–414.

Bluth G. J. S., and Kump L. R. (1994) Lithologic and climatologic controls of river chemistry. *Geochim. Cosmochim. Acta* **58**, 2341–2359.

Bookhagen B., and Burbank D. W. (2006) Topography, relief, and TRMM-derived rainfall variations along the Himalaya. *Geophys. Res. Lett.* **33**, 1–5.

Booth A. L., Zeitler P. K., Kidd W. S. F., Wooden J., Lui Y., Idleman B., Hren M., and Chamberlain C. P. (2004) U–Pb zircon constraints on the tectonic evolution of southeastern Tibet, Namche Barwa area. *Am. J. Sci.* **304**, 889–929.

Burg J. P., and Chen G. M. (1984) Tectonics and structural zonation of southern Tibet, China. *Nature* **311**, 219–223.

Burg J. P., and Meier M. (1997) Exhumation during crustal folding in the Namche-Barwa syntaxis. *Terra Nova* **9**, 53–56.

Burg J. P., Nievergelt P., Oberli F., Seward D., Davy P., Maurin J. C., Diao Z., and Meier M. (1998) The Namche Barwa syntaxis: evidence for exhumation related to compressional crustal folding. *J. Southeast Asian Earth Sci.* **16**, 239–252.

Chamberlain C. P., Koons P. O., Meltzer A. S., Park S. K., Craw D., Zeitler P., and Poage M. A. (2002) Overview of hydrothermal activity associated with active orogenesis and metamorphism: Nanga Parbat, Pakistan Himalaya. *Am. J. Sci.* **302**, 726–748.

Chamberlain C. P., Waldbauer J. R., and Jacobson A. D. (2005) Strontium, hydrothermal systems and steady-state chemical weathering in active mountain belts. *Earth Planet. Sci. Lett.* **238**, 351–366.

Chen C., and Guan Z. (1981) Hydrochemistry of rivers in Xizang. In *Geological and Ecological Studies of Qinghai-Xizang Plateau*, pp. 1687–1692. Science Press, Beijing, Gordon and Breach, New York.

Chou L., Garrels R. M., and Wollast R. (1989) Comparative study of the kinetics and mechanisms of dissolution of carbonate minerals. *Chem. Geol.* **78**, 269–282.

Craw D., Koons P. O., Zeitler P. Z., and Kidd W. S. F. (2005) Fluid evolution and thermal structure in the rapidly exhuming gneiss complex of Namche Barwa-Gyala Peri, eastern Himalayan syntaxis. *J. Metamorph. Geol.* **23**, 829–845.

Dalai T. K., Krishnaswami S., and Sarin M. M. (2002) Major ion chemistry in the headwaters of the Yamuna river system: Chemical weathering, its temperature dependence and CO_2 consumption in the Himalaya. *Geochim. Cosmochim. Acta* **66**, 3397–3416.

Ding L., and Zhong D. (1999) Metamorphic characteristics and tectonic implications of the high-pressure granulites from Namche Barwa, eastern Tibet. *Sci. China.* **42**, 491–505.

Dowling C. B., Poreda R. J., and Basu A. R. (2003) The groundwater geochemistry of the Bengal Basin: Weathering, chemsorption, and trace metal flux to the oceans. *Geochim. Cosmochim. Acta* **67**, 2117–2136.

Drever J. I. (1997) *The Geochemistry of Natural Waters: Surface and Groundwater Environments.* Prentice Hall, New Jersey.

Edmond J. M., and Huh Y. (1997) Chemical weathering yields from basement and orogenic terrains in hot and cold climates. In *Tectonic Uplift and Climate Change*, (ed. W.F. Ruddiman). Plenum Press, New York.

Evans M. J., Derry L. A., Anderson S. P., and France-Lanord C. (2001) Hydrothermal sources of radiogenic Sr to Himalayan rivers. *Geol.* **29**, 803–806.

Evans M. J., Derry L. A., and France-Lanord C. (2004) Geothermal fluxes of alkalinity in the Narayani river system of central Nepal. *Geochem. Geophys. Geosyst.* **5**, 1–21.

Finlayson D. P., Montgomery D. R., and Hallet B. (2002) Spatial coincidence of rapid inferred erosion within young metamorphic massifs in the Himalayas. *Geol.* **30**, 219–222.

Finnegan N., Roe G., Montgomery D. R., and Hallet B. (2005) Controls on the channel width of rivers: Implications for modeling fluvial incision of bedrock. *Geol.* **33**, 229–232.

Gaillardet J., Dupré B., Louvat P., and Allegre C. J. (1999) Global silicate weathering and CO_2 consumption rates deduced from the chemistry of large rivers. *Chem. Geol* **159**, 3–30.

Galy A., and France-Lanord C. (1999) Weathering processes in the Ganges–Brahmaputra basin and the riverine alkalinity budget. *Chem. Geol.* **159**, 31–60.

Galy A., and France-Lanord C. (2001) Higher erosion rates in the Himalaya: geochemical constraints on riverine fluxes. *Geology* **29**, 23–26.

Gansser A. (1964) *Geology of the Himalayas.* Wiley Interscience, London.

Gansser A. (1980) The Significance of the Himalayan Suture Zone. *Tectonophysics* **62**, 37–52.

Garzanti E., Vezzoli G., Andò S., France-Lanord C., Singh S. K., and Foster G. (2004) Sand petrology and focused erosion in focused erosion in collision orogens: the Brahmaputra case. *Earth Planet. Sci. Lett.* **220**, 157–174.

Guan Z., and Chen C. (1981) Hydrographical features of the Yarlung Zangbo river. In *Geological and Ecological Studies of Qinghai-Xizang Plateau*, pp. 1693–1703. Science Press, Beijing, Gordon and BreachNew York.

Harris N., Bickle M. J., Chapman H., Fairchild I., and Bunbury J. (1998) The significance of Himalayan rivers for silicate weathering rates: Evidence from the Bhote Kosi tributary. *Chem. Geol.* **144**, 205–220.

Hasnain S. I., and Thayyen R. J. (1999) Controls on the major-ion chemistry of the Dokriani glacier meltwaters, Ganga Basin, Garhwal Himalaya, India. *J. Glaciol.* **45**, 87–92.

Hui-xin S. (1981) Geochemical characteristics of hot fluids in Xizang. In *Geological and Ecological Studies of Qinghai-Xizang Plateau*, pp. 889–894. Science Press, Beijing, Gordon and Breach, New York.

Jacobson A. D., Blum J. D., and Walter L. M. (2002) Reconciling the elemental and Sr isotope composition of Himalayan weathering fluxes: Insights from the carbonate geochemistry of stream waters. *Geochim. Cosmochim. Acta* **66**, 3417–3429.

Jacobson A. D., Blum J. D., Chamberlain C. P., Craw D., and Koons P. O. (2003) Climatic and tectonic controls on chemical weathering in the New Zealand Southern Alps. *Geochim. Cosmochim. Acta* **67**, 29–46.

Knighton A. D. (1998) *Fluvial Forms and Processes—A New Perspective*. Edward Arnold Ltd, London, 384 pp.

Koons P. O. (1995) Modeling the topographic evolution of collisional mountain belts. Invited paper: *Ann. Rev. Earth Planet. Sci.* **23**, 375–408.

Koons P. O., Craw D., Cox S., Upton P., Templeton A., and Chamberlain C. P. (1998) Fluid flow during active oblique convergence: a Southern Alps model from mechanical and geochemical observations. *Geology* **26**, 159–162.

Krishnaswami S., Singh S. K., Goswami J. N., and Krishnaswami S. (1998) Silicate and carbonate weathering in the drainage basins of the Ganga-Ghaghara-Indus head waters: Contributions to major ion and Sr isotope geochemistry. *Proc. Indian Acad. Sci. (Earth Planet. Sci.)* **107**, 283–291.

Lal D., Harris N. B. W., Sharma K. K., Gu Z., Ding L., Liu T., Dong W., Caffee M. W., and Jull A. J. T. (2003) Erosion history of the Tibetan Plateau since the last interglacial: constraints from the first studies of cosmogenic 10Be from Tibetan bedrock. *Earth Planet. Sci. Lett.* **217**, 33–42.

Li J. J., and Zheng B. X. (1981) The monsoon maritime glaciers in the southeastern part of Xizang. In *Geological and Ecological Studies of Qinghai-Xizang Plateau*, pp. 1599–1610. Science Press, Beijing, Gordon and Breach, New York.

Malloy M. (2004) Rapid erosion at the Tsangpo knickpoint and exhumation of Southeastern Tibet. M.S. Thesis. Lehigh University.

Milliman J. D., and Meade R. H. (1983) World-wide delivery of river sediment to the oceans. *J. Geol.* **91**, 1–21.

Millot R., Gaillardet J., Dupré B., and Allègre C. J. (2002) The global control of silicate weathering rates and the coupling with physical erosion: new insights from rivers of the Canadian Shield. *Earth Planet. Sci. Lett.* **196**, 83–98.

Moore W. S. (1997) High fluxes of radium and barium from the mouth of the Ganges–Brahmaputra river during low river discharge suggest a large groundwater source. *Earth Planet. Sci. Lett.* **150**, 141–150.

Moore D. M., and Reynolds R. C. (1997) *X-ray Diffraction and the Identification and Analysis of Clay Minerals*. Oxford University Press, Oxford.

Mortatti J., and Probst J. L. (2004) Silicate rock weathering and atmospheric/soil CO_2 uptake in the Amazon basin estimated from river water geochemistry: seasonal and spatial variations. *Chem. Geol.* **197**, 177–196.

Niehoff N., Matschullat J., Ruppert H., and Siewers U. (1994) On the chemistry of the precipitation in eastern Tibet (summer 1992). *Geojournal.* **34**, 67–74.

Nijampurkar V. N., Sarin M. M., and Rao D. K. (1993) Chemical composition of snow and ice from Chota Shigri glacier, Central Himalaya. *J. Hydrol.* **151**, 19–34.

Oliva P., Viers J., and Dupre B. (2003) Chemical weathering in granitic environments. *Chem. Geol.* **202**, 225–256.

Pandey S. K., Singh A. K., and Hasnain S. I. (2001) Hydrochemical characteristics of meltwater draining from Pindari glacier, Kumaon Himalaya. *J. Geol Soc. India* **57**, 519–527.

Pascoe E. H. (1963) A Manual of the Geology of India and Burma. vol. 3. Government of India Press, Calcutta, pp. 2073–2079.

Ping Z., Ji D., and Jian J. (2000) A new geochemical model of the Yangbajin geothermal field, *Tibet. Proc. World Geothermal Congress*, 1–6.

Raymo M. E., Ruddiman W. E., and Froelich P. N. (1988) Influence of late Cenozoic mountain building on ocean geochemical cycles. *Geology* **16**, 649–653.

Raymo M. E., and Ruddiman W. F. (1992) Tectonic forcing of late Cenozoic climate. *Nature* **10**, 117–122.

Riebe C. S., Kirchner J. W., Granger D. E., and Finkel R. C. (2001) Strong tectonic and weak climatic control of long-term chemical weathering rates. *Geology* **29**, 511–514.

Riebe C. S., Kirchner J. W., and Finkel R. C. (2004) Erosional and climatic effects on long term chemical weathering rates in granitic landscapes spanning diverse climate regimes. *Earth Planet. Sci. Lett.* **224**, 547–562.

Sarin M. M., and Krishnaswami S. (1984) Major ion chemistry of the Ganga–Brahmaputra river systems, India. *Nature* **312**, 538–541.

Sarin M. M., Krishnaswami S., Dilli K., Somayajulu B. L. K., and Moore W. S. (1989) Major ion chemistry of the Ganga–Brahmaputra river system: Weathering processes and fluxes to the Bay of Bengal. *Geochim. Cosmochim. Acta* **53**, 997–1009.

Satsangi G. S., Lakhani A., Khare P., Singh S. P., Kumari K. M., and Srivastava S. S. (1998) Composition of rain water at a semi-arid rural site in India. *Atm. Environ.* **32**, 3783–3793.

Singh S. K., and France-Lanord C. (2002) Tracing the distribution of erosion in the Brahmaputra watershed from isotopic compositions of stream sediments. *Earth Planet. Sci. Lett.* **202**, 645–662.

Singh S. K., Reisber L., and France-Lanord C. (2003) Re–Os isotope systematics of sediments of the Brahmaputra River system. *Geochim. Cosmochim. Acta* **67**, 4101–4111.

Singh S., Sarin M. M., and France-Lanord C. (2005) Chemical erosion in the eastern Himalaya: major ion composition of the Brahmaputra and $\delta^{13}C$ of dissolved inorganic carbon. *Geochim. Cosmochim. Acta* **69**, 3573–3588.

Si-yu W., and Ji-wen T. (1981) Distribution of geothermal activity and characteristics of geophysical fields on the Xizang plateau. In *Geological and Ecological Studies of Qinghai-Xizang Plateau*, pp. 865–874. Science Press, Beijing, Gordon and Breach, New York.

Smith C. A. S., Clark M., Broll G., Ping C. L., Kimble J. M., and Luo G. (1999) Characterization of selected soils from the Lhasa region of Qinghai-Xizang plateau, SW China. *Permafrost Periglacial Process.* **10**, 211–222.

Stallard R. F., and Edmond J. M. (1981) Geochemistry of the Amazon 1. Precipitation chemistry and the marine contribution to the dissolved load at the time of peak discharge. *J. Geophys. Res.* **86**, 9844–9858.

Vance D., Bickle M., Ivy-Ochs S., and Kubik P. W. (2003) Erosion and exhumation in the Himalaya from cosmogenic isotope inventories of river sediments, *Earth Planet. Sci. Lett.* **206**, 273–288.

Wake C. P., Mayewski P. A., Xie Z., Wang P., and Li Z. (1993) Regional variation of monsoon and desert dust signals recorded in Asian glaciers. *Geophys.Res. Lett.* **20**, 1411–1414.

Wake C. P., Mayewski P. A., Li Z., Han J., and Qin Q. (1994a) Modern eolian dust deposition in central Asia. *Tellus* **46B**, 220–233.

Wake C. P., Dibb J. E., Mayewski P. A., Xie Z., Li Z., Ping W., and Qin D. (1994b) The chemical composition of aerosols over the eastern Himalaya and Tibetan Plateau during low dust periods. *Atmos. Environ.* **28A**, 695–704.

Waldbauer J. R. and Chamberlain C. P. (2005) Influence of uplift, weathering and base cation supply on past and future CO_2 levels. In *A History of Atmospheric CO_2 and its Effects on Plants, Animals and Ecosystems*, Ecological Studies, vol. 177 (eds. J. R. Ehleringer, T. E. Cerling, and M. D. Dearing). Springer, pp. 166–184.

Wei T., and Ming-Tao Z. (1981) Characteristics of geothermal activities in Xizang plateau and their controlling influence on plateau's tectonic model. In *Geological and Ecological Studies of Qinghai-Xizang Plateau*, pp. 841–846. Science Press, Beijing, Gordon and Breach, New York.

West J., Galy A., and Bickle M. (2005) Tectonic and climatic controls on silicate weathering. *Earth Planet. Sci. Lett.* **235**, 211–228.

White A. F., and Blum A. E. (1995) Effects of climate on chemical weathering in watersheds. *Geochim. Cosmochim. Acta* **59**, 1729–1747.

Yin A., and Harrison T. M. (2000) Geologic evolution of the Himalayan-Tibetan orogen. *Ann. Rev. Earth Planet. Sci.* **28**, 211–280.

Zeitler P. K., Chamberlain C. P., and Smith H. A. (1993) Synchronous anatexis, metamorphism, and rapid denudation at Nanga Parbat (Pakistan Himalaya). *Geology* **21**, 347–350.

Zeitler P. K., Melzer A. S., Koons P. O., Craw D., Hallet B., Chamberlain C. P., Kidd W. S. F., Park S. K., Seeber L., Bishop M. P., and Shroder J. F. (2001) Erosion, Himalayan tectonics and the geomorphology of metamorphism. *GSA Today* **11**, 4–8.

Zhang Y., Dai T., and Hong A. (1981) *Isotopic Geochronology of Granitoid Rocks in Southern Xizang Plateau Geological and Ecological Studies of Qinghai-Xizang Plateau.* Science, Science Press, Beijing, Gordon and Breach, New York, 1599–1610.

Zhang D. D., Peart M., Jim C. Y., He Y. Q., Li B. S., and Chen J. AA. (2003) Precipitation chemistry of Lhasa and other remote towns. *Tibet. Atmos. Environ.* **37**, 231–240.

Associate editor: Karen Johannesson